Copper oxide material & device optimization for photovoltaics

Dissertation

Karl Philipp Hering

1. Physikalisches Institut / Justus-Liebig-Universität Gießen

Contents

Contents 1
List of Figures 3
Citations of published work 7
Acknowledgements 9
Chapter 1: Introduction 11
Chapter 2: $Al_{0.11}Ga_{0.89}N$ – Diminishing the conduction band offset 15
Introduction 16
Experimental details 24
Device characterization 25
Conclusion 32
Chapter 3: Cu_2O:H – Passivating Defects 33
Introduction 34
Experimental details 36
Structural properties 38
Electronic transport properties I 40
Hydrogen incorporation 44
Morphological properties 48
Electronic transport properties II 50
Device characterization 56
Conclusion 61
Chapter 4: Semi-transparent electrode – Tuning the plasma 63
Introduction 64
Experimental details 66
Structural properties 68
Electronic transport properties and deposition rate 70
Device characterization 72
Plasma potential measurements 75
Conclusion 76
Chapter 5: Cu_2O:N – Tackling the resistivity 77

Introduction 78
Experimental details 81
Electronic transport properties 82
Conclusion 84
Chapter 6: Summary and future directions 85
References 89

List of Figures

Figure 1: An illustration of the two heterojunction types and the sign convention of the conduction band offset. (left:) A type I heterojunction exhibiting a positive conduction band offset. (right:) A type II heterojunction exhibiting a negative conduction band offset. 17

Figure 2: 1D-Simulation of a n-type window / cuprous oxide heterojunction created with AFORS-HET [15]. In the simulation the conduction band offset was varied. Results of the dependence on that offset are depicted for the main device characterizing values, i.e., open circuit voltage, short circuit current, fill factor and conversion efficiency. The open circuit voltage and fill factor exhibit a linear decrease for negative conduction band offsets and a plateau in the non-negative regime. The short circuit current shows just a slight decrease in the negative, but a strong suppression in the higher positive conduction band offset regime. The fill factor exhibits a similar behavior. The conversion efficiency, calculated as a product of the other two quantities, shows the decrease in the negative and in the higher positive regime of the conduction band offset, as well as the plateau in between. 19

Figure 3: An illustration of the band offsets between zinc oxide and gallium nitride as well as gallium nitride and cuprous oxide determined via x-ray photoelectron spectroscopy (after Kramm et. al. [18]) 22

Figure 4: An illustration of the band edge positions of the aluminum gallium nitride material system, calculated after Vurgaftman et al. [62] [63] 23

Figure 5: An illustration of the photolithographically structured heterojunction solar cell, consisting of a 100 nm Au and a 20 nm Ti / 100 nm Au metal contact, 1 µm cuprous oxide, 250 nm $Al_{0.11}Ga_{0.89}N$:Si and 4.6 µm GaN/SiN/AlGaN/AlN on a polished sapphire substrate. The diameter of the disc-like cuprous oxide structure is 1 mm. 24

Figure 6: Illuminated current-voltage characteristics in the fourth quadrant, for aluminum gallium nitride on cuprous oxide heterojunctions for several aluminum concentrations in the aluminum gallium nitride alloys. An increase in open circuit voltage is observed for increased aluminum content. The short circuit current nearly remains constant, independent of the aluminum content. A voltage dependence of the photocurrent is also observed. 26

Figure 7: Current-voltage characteristics of the best-performing aluminum gallium nitride on cuprous oxide heterojunction of this experiment measured in the dark and under AM1.5 illumination at 100 mW/cm² in the fourth quadrant, the full characteristics are shown logarithmically scaled in the inset. Open circuit voltage, short circuit current, fill factor and consequently the conversion efficiency are far below the maximum

attainable values of Cu_2O. The junction exhibits relatively poor rectification as seen in the dark characteristics depicted in the inset..... 27

Figure 8: An illustration of the resulting band diagram, where the cuprous oxide absorber is on the left and the aluminum gallium nitride window on the right. The resulting heterointerface between the two semiconductors is of type II, exhibiting a large and by convention negative conduction band discontinuity. The thereby enhanced recombination path across the heterojunction is indicated by the red arrow. 29

Figure 9: Temperature dependent measurement of the open circuit voltage (black circles), linear extrapolation of the measured open circuit voltage to 0 K (blue line), temperature dependent cuprous oxide band gap energy (red dashed line) and calculated temperature dependent open circuit voltage corrected for the conduction band offset (black dashed line). The open circuit voltage linearly increases with deceasing device operating temperature, which was extrapolated down to 0 K, intercepting the ordinate at the interface band gap of 1.13 eV. In respect to the band gap of cuprous oxide, the conduction band offset is determined to 1.04 eV. 31

Figure 10: An illustration of the resulting band diagram in p-type semiconductor under the influence of a hole repelling potential barrier, induced by a positively charged grain boundary..... 35

Figure 11: Peak positions obtained for the (111) reflection of the cuprous oxide in the vicinity of 36° as a function of oxygen flow for various substrate temperatures. For lower temperatures the reflections are located at significantly smaller angles, indicating a copper rich deposition of the compound as well as a strained thin film. As the temperature is elevated the position approaches the reference value (dashed line). 39

Figure 12: Room-temperature Hall carrier mobility (bottom) and Hall carrier concentration (top) of Cu_2O films in dependence on the applied oxygen (left) and hydrogen gas flow rate (right) during growth for various substrate temperatures. While the carrier concentration is just slightly influenced, the mobilities show maxima depending on the stoichiometry, tuned by the argon/oxygen ratio, and the hydrogen flow rate applied. The fixed oxygen flow rate chosen in the growth of each hydrogen series is indicated by a star. 42

Figure 13: Comparison of the transport properties of the $Cu_{2\pm\delta}O$ thin films of the highest mobility for growth without added hydrogen (red) and growth with added hydrogen (blue) for the four different substrate temperatures. Hall carrier concentration (top), Hall mobility (center) and resistivity (bottom). At all substrate temperatures the majority carrier mobilities increase by adding hydrogen, while the carrier concentration remains almost unaffected, resulting in significantly lower resistivity values for samples where hydrogen was added during growth. 43

Figure 15: Dependence of the hydrogen concentration (left axis, full circles) and the grain size (right axis, full triangles) on substrate temperature in a series of Cu_2O thin films grown at oxygen and hydrogen flows of 2.8 to 3.5 sccm and 0.2 sccm, respectively. The decrease of the hydrogen concentration with increasing substrate temperature is accompanied by an increase of the grain size. The dotted line represents the detection limit of the SIMS measurement. The inset depicts the resulting hyperbolical dependence of the hydrogen concentration on grain size, indicating that hydrogen is primarily located at surfaces. 47

Figure 16: Scanning electron microscopy (SEM) images of the surfaces of Cu_2O thin films sputtered at 925 K using different hydrogen flows in the growth process (increasing from top left to bottom right). The oxygen flow was set to 3.3 sccm. The presence of hydrogen in the growth process strongly influences the film morphology; in particular, large grains and disrupted film morphology are induced at elevated flows. 49

Figure 14: Temperature dependent Hall effect measurements of selected samples grown at a substrate temperature of 925 K, i.e., 0, 0.05 and 0.10 sccm, where the effect of hydrogen induced grain growth is negligible. Depicted on the left is the Hall mobility, which has been modeled as a combination of ionized impurity scattering, metastable self-trapping of holes and scattering at grain boundaries (dashed lines). For each data set all parameters are kept constant except the height of the grain boundary barrier ΦB and the density of ionized defects, which was extracted from fitting the carrier concentrations (right) with the standard model for a compensated semiconductor with a single acceptor (dashed lines). The inset of the left graph depicts the temperature dependence of the contributions of the three dominant scattering processes to the total Hall mobility. 55

Figure 17: A comparison of the external quantum efficiencies for both, $Al_{0.11}Ga_{0.89}N$ / Cu_2O heterostructures with (blue) and without (red) the application of hydrogen during the copper oxide deposition. (right) A comparison between illuminated J-V characteristics of the heterostructure employing hydrogen in the deposition process (blue) and without the use of hydrogen (red). 57

Figure 18: For the device employing hydrogen: (left) $J_{SC} - V_{OC}$ characteristics (black), illuminated J-V characteristics shifted by a J_{SC} (dashed), results from curve fitting the diode model without series resistances for a low and high voltage regime to the $J_{SC} - V_{OC}$ curve (red and blue) and results of fitting the diode model including series resistance and parameters extracted from the high voltage regime to the shifted illuminated J-V characteristics in the range of V_{OC} , where the voltage-dependent change in photocurrent is low and the illumination is close to regular operation condition. (right) J-V characteristics in the dark and under illumination. 60

Figure 19: A schematic of the modified deposition setup. The biased grid is located 10 mm above the substrate holder. 67

Figure 20: X-ray diffraction results showing the (111) reflection of cuprous oxide in the vicinity of 36° for samples without a grid (top) and with a biased grid present during the deposition. (insets) Corresponding images of the deposited thin films obtained by scanning electron microscopy..... 69

Figure 21: (top:) Results obtained for the deposition rate in dependence on the applied grid bias. The rate is significantly larger when no grid is present (dashed line). (bottom:) Electrical transport properties measured by Hall effect, i.e., carrier concentration, mobility and specific resistivity (top to bottom), of the deposited thin films in dependence on the applied grid bias. Results of the reference sample without a grid are indicated by the dashed lines. 71

Figure 22: (left:) External quantum efficiency measurements of $Al_{0.11}Ga_{0.89}N$ / Cu_2O heterostructures. The reference is depicted by the dashed line. (top right:) J-V characteristics measured in the dark. (bottom right:) AM1.5 illuminated J-V characteristics in the fourth quadrant..... 73

Figure 23: Measured voltage in dependence on the distance to the grid during the deposition process for several positive grid biases. The grid and substrate holder are located at 0 mm and -10 mm, respectively. The voltage curves exhibit a step when crossing the grid..... 75

Figure 24: Hall carrier concentration (red), specific resistivity (black) and activation energy (black, determined by temperature dependent measurements) in dependence on the nitrogen gas flow rate applied during deposition. The Hall carrier concentration is increasing and specific resistivity as well as activation energy are decreasing with the nitrogen gas flow rate. The dependencies demonstrate excessive acceptor doping taking place by nitrogen incorporation and at higher nitrogen flows a defect band is beginning to form and the electric transport of the cuprous oxide thin film becomes degenerate. 83

Citations of published work

K. P. Hering, J. Benz, C. Kandzia, B. Kramm, M.Eickhoff, and P. J. Klar. *Hydrogen induced mobility enhancement in RF sputtered Cu_2O thin films,* submitted to Advanced Materials

K. P. Hering, and P. J. Klar. *Hydrogen induced efficiency enhancement in $Al_{0.11}Ga_{0.89}N/Cu_2O$ solar cells*, submitted to Applied Physics Letters

J. Hennemann, K. P. Hering, C. Kandzia, and B. Smarsly. *Improved hydrogen sulfide gas sensors based on copper oxide by morphological control*, in preparation

K. P. Hering, R. Bergert, S. Mitic. *Enhanced $A_{11}Ga_{89}N/Cu_2O$ solar cells by a semitransparent electrode,* submitted to Applied Physics Letters

F. Klein, R. Pinedo, K. P. Hering, A. Polity, J. Janek, and P. Adelhelm. *Reaction mechanism and surface film formation of conversion materials for lithium- and sodium-ion batteries: A XPS case study on sputtered copper oxide (CuO) thin film model electrodes,* submitted to J. of Physical Chemistry

D. Hartung, F. Gather, P. Hering, C. Kandzia, D. Reppin, A. Polity, B. K. Meyer, and P. J. Klar. *Assessing the thermoelectric properties of Cu_xO ($x = 1$ to 2) thin films as a function of composition*, Appl. Phys. Lett. 106, 253901 (2015).

K. P. Hering, R. E. Brandt, B. Kramm, T. Buonassisi, and B. K. Meyer, *GaN/Cu_2O Heterojunctions for Photovoltaic Applications*, Energy Procedia 44:32–36 (2014).

K. P. Hering, A. Polity, B. Kramm, A. Portz, and B. K. Meyer, *Synthesis and Characterization of Copper Oxide Compounds*, MRS Symp. Proc. 1633:3-12 (2014).

B. K. Meyer, A. Polity, D. Reppin, M. Becker, P. Hering, P. J. Klar, Th. Sander, C. Reindl, C. Heiliger, M. Heinemann, C. Müller, and C. Ronning. *Chapter 6: The Physics of Copper Oxide (Cu_2O)*, Semiconductors and Semimetals 88:201-226 (2013)

B. K. Meyer, A. Polity, D. Reppin, M. Becker, P. Hering, P. J. Klar, Th. Sander, C. Reindl, J. Benz, M. Eickhoff, C. Heiliger, M. Heinemann, J. Bläsing, A. Krost, S. Shokovets, C. Müller and C. Ronning. *Binary copper oxide semiconductors: From materials towards devices*, Phys. Stat. Sol. (b) 249(8):1487-1509 (2012).

B. Kramm, A. Laufer, D. Reppin, A. Kronenberger, P. Hering, A. Polity, and B. K. Meyer. *The band alignment of Cu_2O/ZnO and Cu_2O/GaN heterostructures*, J. Appl. Phys. Lett. 100:094102 (2012)

Acknowledgements

I would like to express my gratitude to a number of people for their support during my time at the IPI:

Prof. Dr. Bruno Meyer, Prof. Dr. Peter Klar, Prof. Dr. Slobodan Mitic

Prof. Dr. Detlev Hofmann, Prof. Dr. Dietrich Schwabe, Prof. Dr. Jürgen Janek

Prof. Dr. Christian Heiliger, Prof. Dr. Derck Schlettwein, Prof. Dr. Martin Eickhoff

Dr. Angelika Polity, Dr. Torsten Henning, Dr. Stefan Lautenschläger,

Dr. Christian Neumann, Dr. Daniel Reppin, Dr. Boris Mogwitz

Dr. Yinmei Lu, Dr. Marc Dietrich, Dr. Achim Kronenberger

Benedikt Kramm, Julian Benz, Christian Kandzia,

Martin Becker, Philipp Schurig, Melanie Pinnisch,

Jan Philipps, Gunther Haas, Andre Portz,

Gesche Müntze, Katharina Huhn, Waldemar Gärtner,

Peter Köhler, Maria Smirnova

Thomas Nimmerfroh, Hans-Peter Jorde, Felix Herzberger, Norbert Kurmann,

Björn Bellof, Christian Schinz, Yu Lin, Karl Laudenbach, Rene Schubert,

Jürgen Weis, Udo Bachmann, Renate Fuchs and Anja Denhardt

Thank You !

Chapter 1: Introduction

As today's energy consumption is on its all-time high and a further increase is to be expected, limited resources and environmental hazards of fossil fuels require alternative ways to satisfy the energy demand. Photovoltaic conversion of sunlight presents itself as one of the most potent pathways among the alternative technologies presently available, and cost efficiency of the well-established crystalline silicon based technology has been increased significantly. Nevertheless, thick layers of several $10\ \mu m$ are still required for a standard silicon solar-cell due to its indirect band gap and the resulting low optical absorption coefficient in the visible spectral range. Thus, thin-film photovoltaics based on crystalline silicon is a contradiction in terms. Thin-film photovoltaics based on materials composed of sustainable chemical elements may turn out to be more cost efficient in the long run, as they are potentially more energy efficient in the fabrication process and require less active material. Commercially available CIGS and CdTe solar cells demonstrate the potential of thin-film technologies to challenge silicon photovoltaics. In these devices already significantly less active material is used, but still they rely on scarce chemical elements such as In or Te and, in case of CdTe, on toxic Cd. In order to ensure sustainability and environment friendliness, those elements have to be avoided, bringing other material compounds into the focus of research. [1] [2] [3] Among the various candidates with promising potential for application in photovoltaics is cuprous oxide, an intrinsic p-type, nontoxic, and abundant semiconductor material. Recently there has been a revival of research interest in cuprous oxide based photovoltaics, peaking in cell efficiencies beyond 6 %. [4] [5] [6] [7] However, that involved highly crystalline material, obtained from thermally oxidized copper

sheets. To increase cost efficiency a thin-film deposition process with mass production capabilities, yielding material approaching in quality that obtained by thermal oxidation, has to be found. Thin films prepared by sputter deposition or electrodeposition offer low production costs but usually lack crystallinity, and consequently exhibit deficiencies in optoelectronic and transport properties, especially when grown at lower substrate temperatures. [8] [9] [10] [11] [12] Ways to improve material quality need to be sought.

This study is aiming primarily at improving cuprous oxide based photovoltaic devices by identifying and overcoming performance-limiting loss mechanisms. As solar cells are highly sophisticated semiconductor devices, which are very sensitive to numerous influences, one should address major material and device flaws before optimizing the device in terms of, e.g., light management. Thus, this study is focused mainly on the fundamental optimization of the cuprous oxide thin films and the device by tuning the deposition process and the device design by a choice of the heterojunction partner material.

In Chapter 2, the device performance-limiting effect of the conduction band offset is explained and experimentally addressed by the choice of aluminum gallium nitride as the window layer. It is demonstrated that the device performance, especially the open circuit voltage, is increased, when the conduction band offset is lowered by changing the stoichiometry to a higher aluminum content.

In Chapter 3, the successful attempt to passivate defects in the sputtered cuprous oxide thin films by hydrogen and hence to improve the collection length in photovoltaic devices is demonstrated. As the role and passivating effect of hydrogen in the cuprous

oxide thin films was unclear, it gave rise to further investigation, which unveiled a hydrogen induced passivation of donor like defects, that are located at the polycrystalline material's grain boundaries.

In Chapter 4, without the ability to correct the doping profile of the device, the limiting mechanism of strong interface recombination was diminished by a successful attempt to modify the sputter deposition by introducing a semi-transparent electrode. The modification either allows one to lower the electron temperature in the plasma, and thus to assist the desired plasma chemical reaction, or it may be used to reduce the kinetic energy of the ionized atoms and molecules impinging on the aluminum gallium nitride templates, and thus to reduce the sputter deposition induced damage, resulting in a suspected reduction of the interface defect density.

In Chapter 5, the ability to vastly increase the conductivity up to the degeneracy of cuprous oxide by extrinsic doping with acceptors, i.e., the introducing nitrogen gas to the deposition process, is demonstrated. Since the acceptor density in the sputter deposited cuprous oxide thin films is rather too high, an additionally acceptor doped cuprous oxide layer may not help to reduce the currently limiting effects of interface recombination and low collection length, but it may, in a future perspective, be applied to allow for a reduction in production cost, a more sustainable choice of electrode metal as well as a viable solution to suppress recombination at the back contact by introducing a back surface field, thus reducing the electron carrier density.

Chapter 2: $Al_{0.11}Ga_{0.89}N$ – Diminishing the conduction band offset

Content of this Chapter has been published in peer reviewed scientific journals and literature:

K.P. Hering, A. Polity, B. Kramm, A. Portz and B.K. Meyer, *Synthesis and Characterization of Copper Oxide Compounds*, MRS Symp. Proc. 1633:3-12 (2014).

K.P. Hering, R.E. Brandt, B. Kramm, T. Buonassisi and B.K. Meyer, *GaN/Cu_2O Heterojunctions for Photovoltaic Applications*, Energy Procedia 44:32–36 (2014).

K.P. Hering and P.J. Klar, *Hydrogen induced efficiency enhancement in $Al_{0.11}Ga_{0.89}N/Cu_2O$ solar cells*, submitted to Applied physics letters

---

Heterojunction solar cells are very sensitive to the band alignment, as the latter governs the carrier transport, carrier recombination, and Fermi level splitting. Most critical influence on the device performance is exerted by the doping profile of the heterojunction, as it is crucial to create a so-called type inversion of the absorber at the heterointerface, which will lower defect related recombination. For recombination across the interface, this process is activated by the effective band gap energy at the interface, which, in comparison to the absorber band gap, is reduced by the conduction band offset in the case of a type-II heterojunction. It is needless to state that such a conduction band offset impedes the successful type inversion. Moreover, the voltage generated by the heterojunction during photovoltaic operation will be reduced, since not only the energetic position of the Fermi level but also the quasi-Fermi level splitting will be subject to a limitation by a negative conduction band offset. A band offset can be changed by interface dipoles and which by some extent may be used for band offset engineering. In reality though, gaining control over the band alignment at the interface in this fashion usually proves to be impractical, and the only viable option left is the suitable choice of a heterojunction partner material, which is the subject of this Chapter. It is demonstrated that by reducing the conduction band offset to cuprous oxide via alloying gallium nitride, i.e., the window layer, with aluminum, the photovoltaic conversion efficiency is improved significantly.

Introduction

Depending on the respective electron affinities, the heterojunction is classified as type-I, when both, the conduction and valence band edge of one heterojunction partner material energetically lie within the band gap of the other, or type-II, when just the conduction band edge of one material and just the valence band edge of the other are located in the respective partner's band gap, see Figure 1.

As the heterointerface represents an abrupt change in structure and composition of the material, there usually is a large quantity of defects located at its position. This situation gives rise to enhanced defect related recombination, i.e., Shockley-Read-Hall recombination [13] [14], which is usually referred to as interface recombination. This particular recombination process involves four different carrier densities at the interface, i.e., those of electrons and holes in the window and absorber layer, respectively. When interface recombination is dominating, the heterojunction's diode current density, more precisely, the saturation current density, is activated by the interface band gap energy, which represents recombination across the heterointerface of abundant electrons in the window layer with abundant holes in the absorber layer. In the case of a type-I heterojunction solar cell, the interface band gap energy equals the absorber band gap energy. In a type-II junction however, the interface band gap energy equals the absorber band gap energy reduced by the conduction band offset. Thus, a, by convention negative, conduction band offset enhances interface recombination.

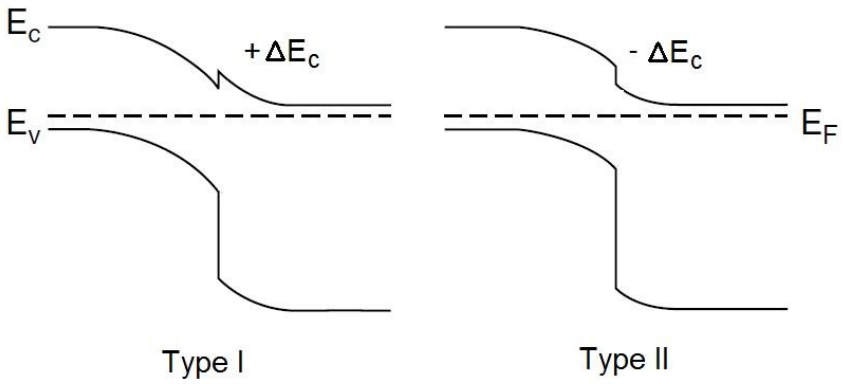

Figure 1: An illustration of the two heterojunction types and the sign convention of the conduction band offset. (left:) A type I heterojunction exhibiting a positive conduction band offset. (right:) A type II heterojunction exhibiting a negative conduction band offset.

Luckily, the sensitivity of the heterojunction to that recombination process can be reduced by the so called type inversion at the heterointerface. In the case of a p-type absorber, that means that the Fermi level has to be located close to the absorber's conduction band edge, so that electrons no longer are minority carriers, or in other terms, holes are no longer abundant in the vicinity of the heterointerface, so that the recombination process, requiring an abundance of both, electrons and holes in the vicinity of the defects, is significantly reduced. That can be achieved by an asymmetric doping profile of the heterojunction, i.e., a situation where the donor density of the window layer is significantly larger than the acceptor density of the absorber layer. Consequently, band bending will mainly take place in the absorber, as its space charge region is extended so that, at the interface, the Fermi level is elevated to the absorber's conduction band edge.

However, in a non–degenerate case, the Fermi level position is limited by the resulting interface band gap and consequently, the quasi-Fermi level splitting under illumination

is limited also. Therefore, a negative conduction band offset not only enhances interface recombination but also prevents a possible type inversion and limits the attainable open circuit voltage. The latter becomes more evident when the voltage generated by the illuminated solar cell is expressed in terms of quasi-Fermi level splitting, i.e.,

$$qV = E_{F_n} - E_{F_p} \quad (1)$$

The dependence of the main device characteristics, i.e., open circuit voltage, short circuit current density, fill factor, and the photovoltaic conversion efficiency, on the conduction band offset was simulated with the 1D-simulation program AFORS-HET [15]; results are depicted in Figure 2. The parameters used in the simulation are a virtual window layer, exhibiting a band gap of 3.4 eV to ensure transparency with respect to the solar spectrum and a donor density of 1E18 cm^{-3} exhibiting a doping efficiency of 100 %, i.e., $N_d = n$. The cuprous oxide band gap was set to 2 eV and the acceptor density to 1E16 cm^{-3} at an energy of 200 meV above the valence band. The absorption coefficient of the window layer is set to zero, and that of cuprous oxide is taken from the work of Meyer et al. [8]. Reflection losses at the front were set to a realistic value of 20 % and transmission losses as well as interference effects disregarded. Interface recombination was included by a discrete defect level located in the middle of the interface band gap.

For negative conduction band offsets, the open circuit voltage is decreased as discussed above, on approaching a conduction band alignment between the two semiconductors and for non-negative conduction band offsets, the open circuit voltage exhibits a plateau. That is explained by the fact that the quasi Fermi level splitting is now limited by the full

absorber band gap, since the conduction band offset will no longer reduce the interface band gap, when entering the positive regime.

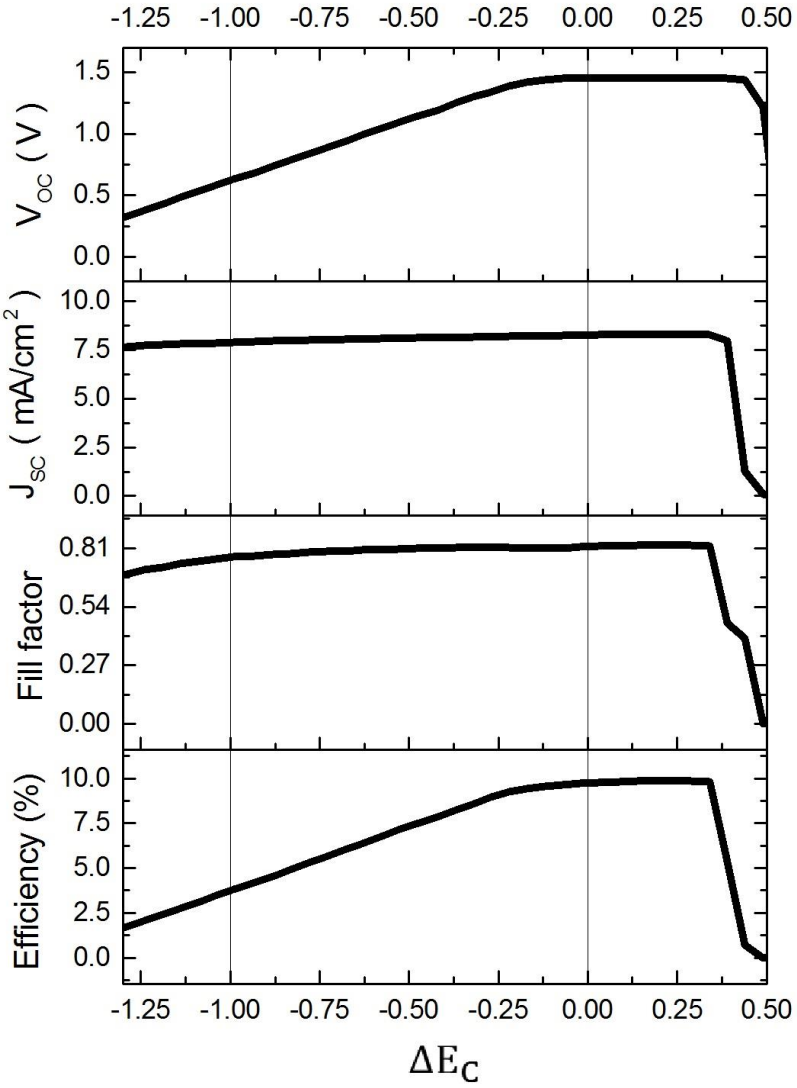

Figure 2: 1D-Simulation of a n-type window / cuprous oxide heterojunction created with AFORS-HET [15]. In the simulation the conduction band offset was varied. Results of the dependence on that offset are depicted for the main device characterizing values, i.e., open circuit voltage, short circuit current, fill factor and conversion efficiency. The open circuit voltage and fill factor exhibit a linear decrease for negative conduction band offsets and a plateau in the non-negative regime. The short circuit current shows just a slight decrease in the negative, but a strong suppression in the higher positive conduction band offset regime. The fill factor exhibits a similar behavior. The conversion efficiency, calculated as a product of the other two quantities, shows the decrease in the negative and in the higher positive regime of the conduction band offset, as well as the plateau in between.

The short circuit current density slightly decreases for negative conduction band offsets. The sensitivity of the dependence of this current density on the conduction band offset is controlled by the interface recombination velocity, which scales directly with the density of interface defects. In addition, the carrier densities at the interface play a role, which are controlled by the doping profile of the heterojunction. Also the short circuit current density exhibits a plateau entering the positive conduction band offset regime. For values exceeding 0.4 eV, the current is suppressed. This suppression is due to the fact that a positive conduction band offset introduces a potential barrier for the photogenerated electron current directed across the heterojunction, which is surmounted via thermionic emission. Thus the photogenerated current is now facing a limitation by the maximum current density that is supported by the thermionic emission process. The latter is dependent on the barrier height, i.e., the conduction band offset. Exceeding 0.4 eV, the limitation will become dominant, so that the photogenerated electron current and consequently, the short circuit current density is suppressed.

In an idealized case, one may express the fill factor in terms of open circuit voltage and ideality factor of the diode only. To understand the dependence of the fill factor in the non-ideal case including band offsets and interface recombination one has to consider the arguments given above at a forward-biased heterojunction. Disregarding parasitic resistances, the diode current is given by the ideal Shockley equation. [16]

$$J = J_s\left(e^{-\frac{qV}{nkT}} - 1\right) \tag{2}$$

At negative conduction band offsets the saturation current density is large, and the slope of the exponential bias dependence is amplified, resulting in a less steep incline of the

current towards the open circuit condition, so that the current-voltage characteristics in the fourth quadrant becomes less rectangular. Consequently, the fill factor is reduced. On entering the positive regime of the conduction band offset, the saturation current density will not change, thus the fill factor remains constant. In the limit of thermionic emission, the ratio of diode current to photogenerated current is increasing with the conduction band offset. Therefore, the impact of the diode current is increased and again the steepness of the current-voltage characteristics is reduced.

The dependence of the conversion efficiency may be explained by the dependencies stated above, as it is calculated as the product of open circuit voltage, short circuit current density, and fill factor, divided by the irradiance. Therefore, a positive conduction band offset exceeding 0.4 eV, or a negative conduction band offset will reduce the efficiency.

In summary, a positive conduction band offset exceeding 0.4 eV, as well as a negative conduction band offset in any extent are diminishing a heterojunction solar cell's conversion efficiency and have to be avoided by all means.

For a more detailed presentation on the influence of the conduction band offset on a heterojunction solar cell, the interested reader is referred to the work of R. Scheer and H.-W. Schock [17], forming the basis for the explanations given above.

In case of cuprous oxide, the challenge is to find a suitable heterojunction partner material, which is by definition required to exhibit strong n-type conductivity and a band gap granting sufficient transparency to the solar spectrum, in order to place photogeneration within the space charge region. Suitable materials prove to be scarce considering the small electron affinity of cuprous oxide.

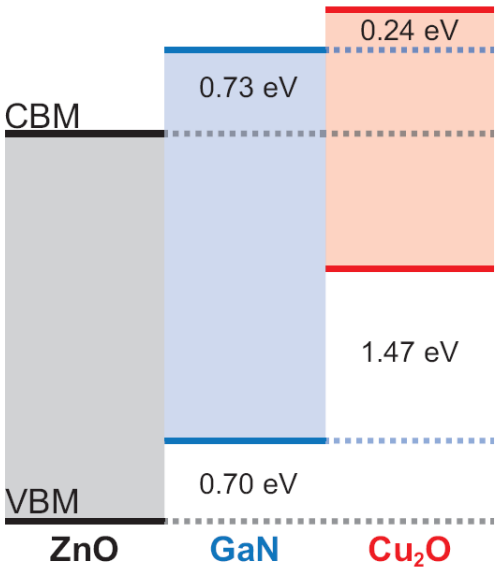

Figure 3: An illustration of the band offsets between zinc oxide and gallium nitride as well as gallium nitride and cuprous oxide determined via x-ray photoelectron spectroscopy (after Kramm et. al. [18])

Following the findings of Kramm et al. [18], who determined the conduction band offset between gallium nitride and cuprous oxide to -0.24 eV, the aluminum gallium nitride material system presents itself as meeting those requirements, being scientifically well understood, technologically applied and thus available. Furthermore, GaN offers the possibility to tune the energetic conduction band edge position by merely varying stoichiometry by adding aluminum, as illustrated in Figure 3. Although less sustainable, the alloy system (Al,Ga)N was applied in this thesis as window material and can be understood as a place holder until a more sustainable and environment friendly material as a suitable replacement is discovered.

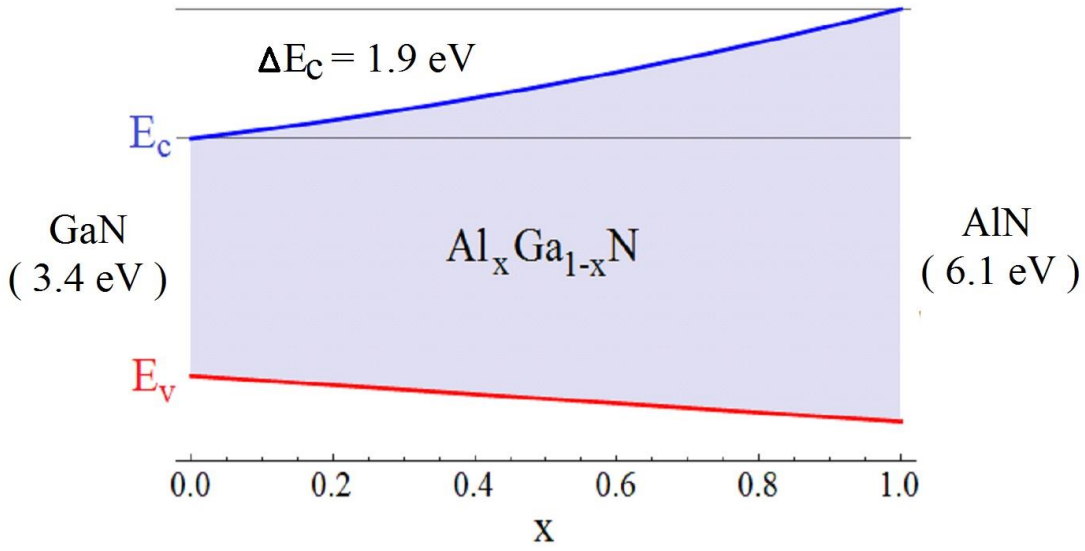

Figure4: An illustration of the band edge positions of the aluminum gallium nitride material system, calculated after Vurgaftman et al. [62] [63]

Experimental details

The cuprous oxide thin films were prepared by RF sputtering on n-type (aluminum) gallium nitride templates, $N_d \approx 2E17\ cm^3$, kindly provided by Dr. A. Dadgar and Prof. A. Krost [19]. Argon with controlled admixtures of oxygen was used as working gas. The vacuum environment was purged with argon and evacuated to a pressure of at least $5 \cdot 10^{-6}$ mbar prior to deposition. By adjusting the gas flows, the working pressure was set to $8 \cdot 10^{-3}$ mbar and RF power kept constant at 50 W. The substrate holder was heated to 925 K. The deposition time was chosen to yield film thicknesses of 1 µm. The deposition was followed up by photolithographic structuring, thermal evaporation, and annealing of metal contacts, i.e., Ti/Au for the template and Au for the cuprous oxide absorber [20], and ultrasonic wire bonding, as illustrated in Figure 4. Current-voltage characteristics were recorded with a Keithley SCS4200 system, Oriel Xe arc lamp and AM1.5 filter.

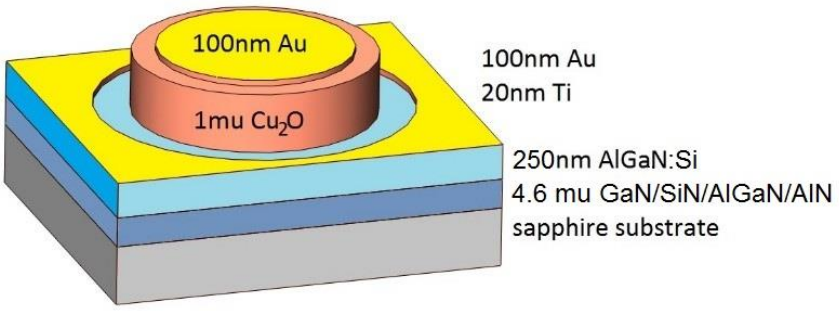

Figure 5: An illustration of the photolithographically structured heterojunction solar cell, consisting of a 100 nm Au and a 20 nm Ti / 100 nm Au metal contact, 1 **µm** cuprous oxide, 250 nm $Al_{0.11}Ga_{0.89}N$:Si and 4.6 **µm** GaN/SiN/AlGaN/AlN on a polished sapphire substrate. The diameter of the disc-like cuprous oxide structure is 1 mm.

Device characterization

Depicted in Figure 5 are the Am1.5 illuminated current-voltage characteristics in the fourth quadrant for heterojunctions of cuprous oxide on aluminum gallium nitride templates, exhibiting different aluminum concentrations. The short circuit current remains almost constant, while the open circuit voltage is clearly increased for higher aluminum concentrations. In addition, the finding that the cuprous oxide thin film is being 'excessively' doped by intrinsic acceptors, as discussed in more detail in Chapter 3, results in a non-optimized doping profile, which ultimately enhances interface recombination by an absent type inversion at the absorber interface, as discussed in the introduction of this Chapter. Also, it causes a space charge region which does not extend far into the absorber layer. In conjunction with minority carrier lifetimes being too low to compensate this effect, that is responsible for the significantly lowered short circuit current. Also, characteristic for a low $\mu\tau$ product is a lowered and strongly voltage dependent photocurrent in the current-voltage characteristics, which is observed in the experiment.

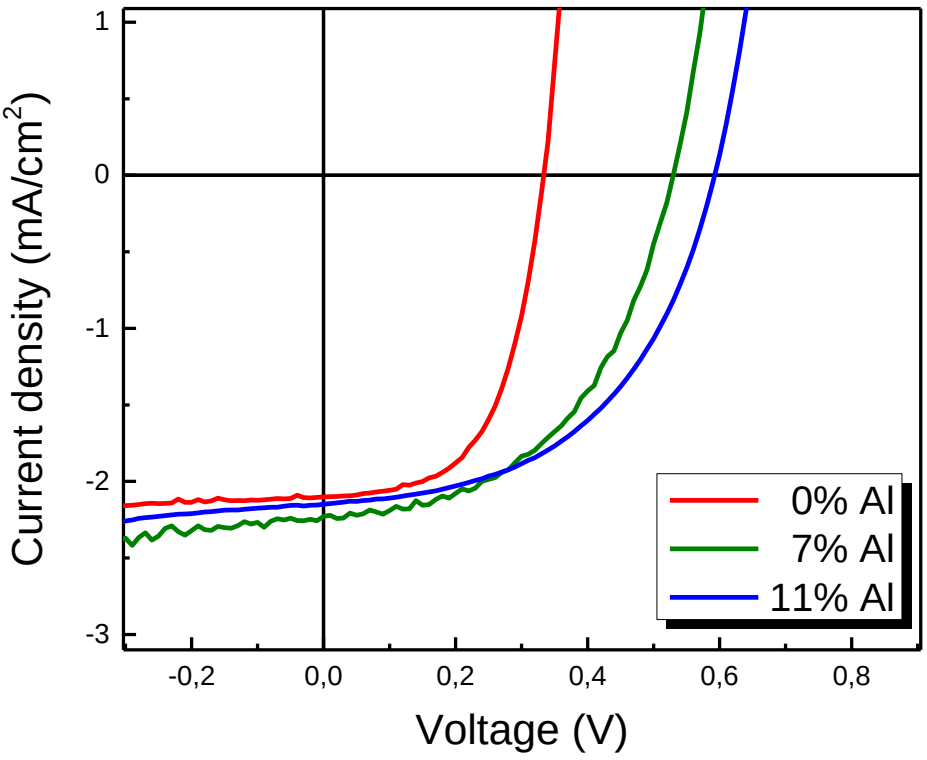

Figure 6: Illuminated current-voltage characteristics in the fourth quadrant, for aluminum gallium nitride on cuprous oxide heterojunctions for several aluminum concentrations in the aluminum gallium nitride alloys. An increase in open circuit voltage is observed for increased aluminum content. The short circuit current nearly remains constant, independent of the aluminum content. A voltage dependence of the photocurrent is also observed.

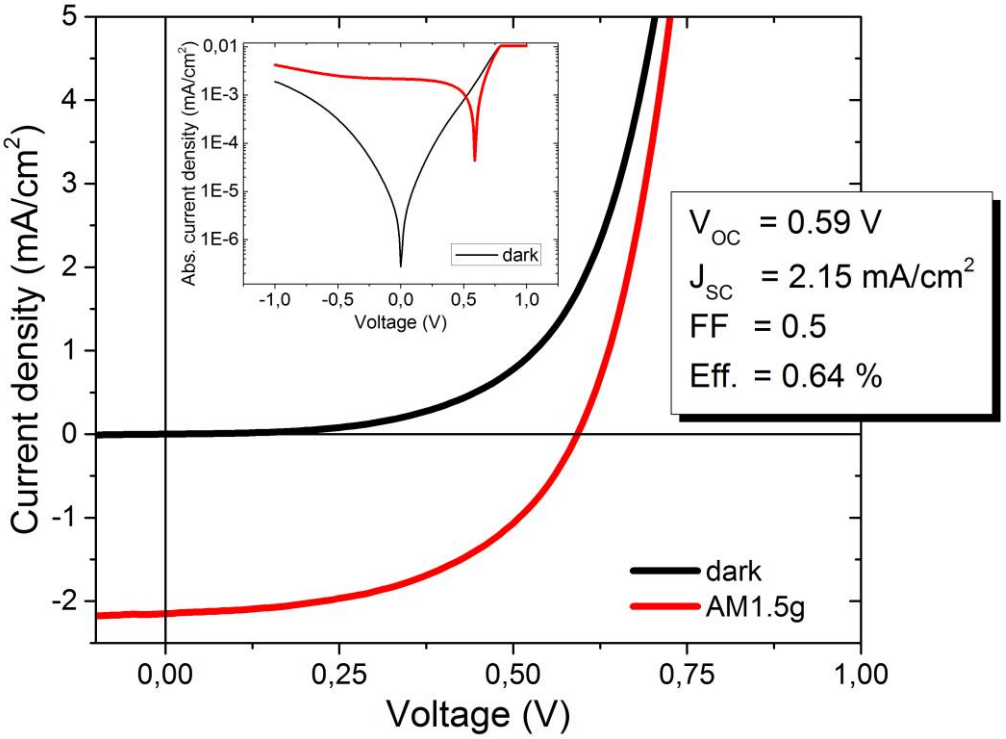

Figure 7: Current-voltage characteristics of the best-performing aluminum gallium nitride on cuprous oxide heterojunction of this experiment measured in the dark and under AM1.5 illumination at 100 mW/cm² in the fourth quadrant, the full characteristics are shown logarithmically scaled in the inset. Open circuit voltage, short circuit current, fill factor and consequently the conversion efficiency are far below the maximum attainable values of Cu_2O. The junction exhibits relatively poor rectification as seen in the dark characteristics depicted in the inset.

The current- voltage characteristics measured in the dark and under AM1.5 illumination of the best-performing heterojunction involving $Al_{0.11}Ga_{0.89}N$ is shown in Figure 6. As the band gap of cuprous oxide is roughly 2 eV at room temperature, an open circuit voltage significantly larger than that one observed in this experiment can be expected. A possible origin of the reduced open circuit voltage may be a negative and rather large conduction band offset between the cuprous oxide absorber and the underlying aluminum gallium nitride template, as illustrated in Figure 7, limiting the built-in bias or in other terms effectively reducing the activation energy of the diode saturation current, i.e., a reduction from the absorber band gap energy down to the 'effective' band gap energy at the interface between the aluminum gallium nitride window conduction band edge and the cuprous oxide absorber valence band edge. Since such a conduction band offset also enhances interface recombination across the heterojunction. Interface recombination is strong when the ratio between the window and absorber doping densities N_d/N_a is not sufficiently large. In reference to the work of Lee et al. [9], the application of gallium oxide in a heterostructure with cuprous oxide leads to a large open circuit voltage of 1.2 V. In that work the temperature dependent measurements of the open circuit voltages allow the authors to determine the effective band gap by extrapolation. They found that the effective band gap is approaching almost the full energy of the absorber band gap at 0 K. As the photocurrent of that device is not suppressed, the conduction band edges of the two semiconductors, i.e., gallium oxide and cuprous oxide, must be close to alignment. Estimations of the conduction band offset based on XPS measurements and optical band gaps determined by transmission spectra have been attempted, yielding a large

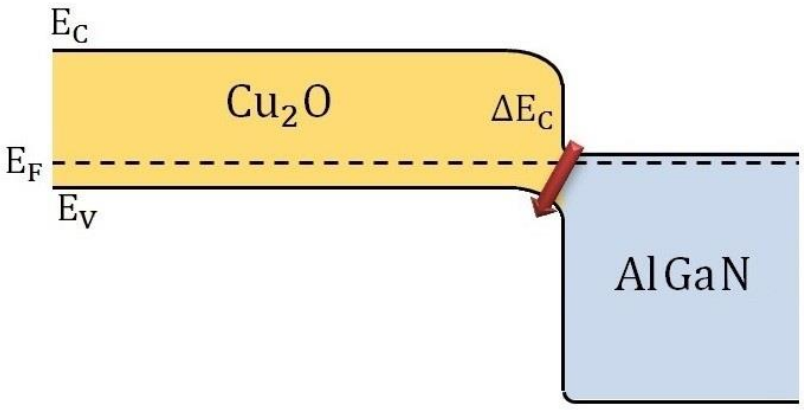

Figure 8: An illustration of the resulting band diagram, where the cuprous oxide absorber is on the left and the aluminum gallium nitride window on the right. The resulting heterointerface between the two semiconductors is of type II, exhibiting a large and by convention negative conduction band discontinuity. The thereby enhanced recombination path across the heterojunction is indicated by the red arrow.

discrepancy in the results, i.e., values ranging from -0.34 eV to +0.5 eV, including measurement errors. [21] [10] The conduction band offset between gallium nitride and cuprous oxide thin films of -0.24 eV, determined in that manner by Kramm et al [18], appears to be largely underestimated with respect to the findings of this experiment. Assuming a reduction of the open circuit voltage by $\Delta E_C/q$ and a conservative conduction band offset of -0.2 eV for the Ga_2O_3 / Cu_2O heterojunction, in relation to the open circuit voltage of 1.2 V observed by Lee et al, the offset in this experiment may be estimated to -1.0 eV to -0.8 eV, for GaN to $Al_{0.11}Ga_{0.89}N$. When applying the transitivity rule and allowing for measurement errors of 0.15 eV, this estimation is backed by the XPS based findings of You et al. [22] who determined the conduction band offset between zinc oxide and gallium nitride to be -0.15 eV, and of Brandt et al. [21], who determined a value of -1.34 eV for the conduction band offset between zinc oxide and cuprous oxide. However, as already indicated above, an XPS based analysis of band

offsets is prone to enormous errors from the point of view of device engineering and therefore in my opinion somewhat unreliable and misleading.

In order to investigate the suspected large negative conduction band offset, one may collect data on the temperature dependence of the open circuit voltage, as already stated above. The temperature dependent measurement allows one to directly determine the energy in the band diagram that limits the open circuit voltage by a simple linear extrapolation to zero Kelvin, where all other voltage reducing factors are disabled due to their temperature dependence as long as the Fermi level is not pinned by defects. The latter can be distinguished by a temperature independent open circuit voltage. In the case where the open circuit voltage is extrapolated to an energy corresponding voltage less than the absorber band gap, it is the direct proof and determination of the suspected negative conduction band offset of the heterojunction solar cell. Obviously, this method can only be applied to determine negative conduction band offsets in a type-II heterojunction. In order to be able to directly compare to the value of -0.24 eV of Kramm et al., the measurement was carried out for the gallium nitride / cuprous oxide device. Indeed, the suspected attributes and estimated higher value of the conduction band offset are validated by the measurement depicted in Figure 5. It is found that the actual conduction band offset of this gallium nitride / cuprous oxide heterojunction is roughly -1 eV. Also, a virtual open circuit voltage was calculated by correcting for the determined conduction band offset, and assuming an identical temperature dependence to illustrate the performance of a cuprous oxide based solar cell exhibiting a proper flat band alignment.

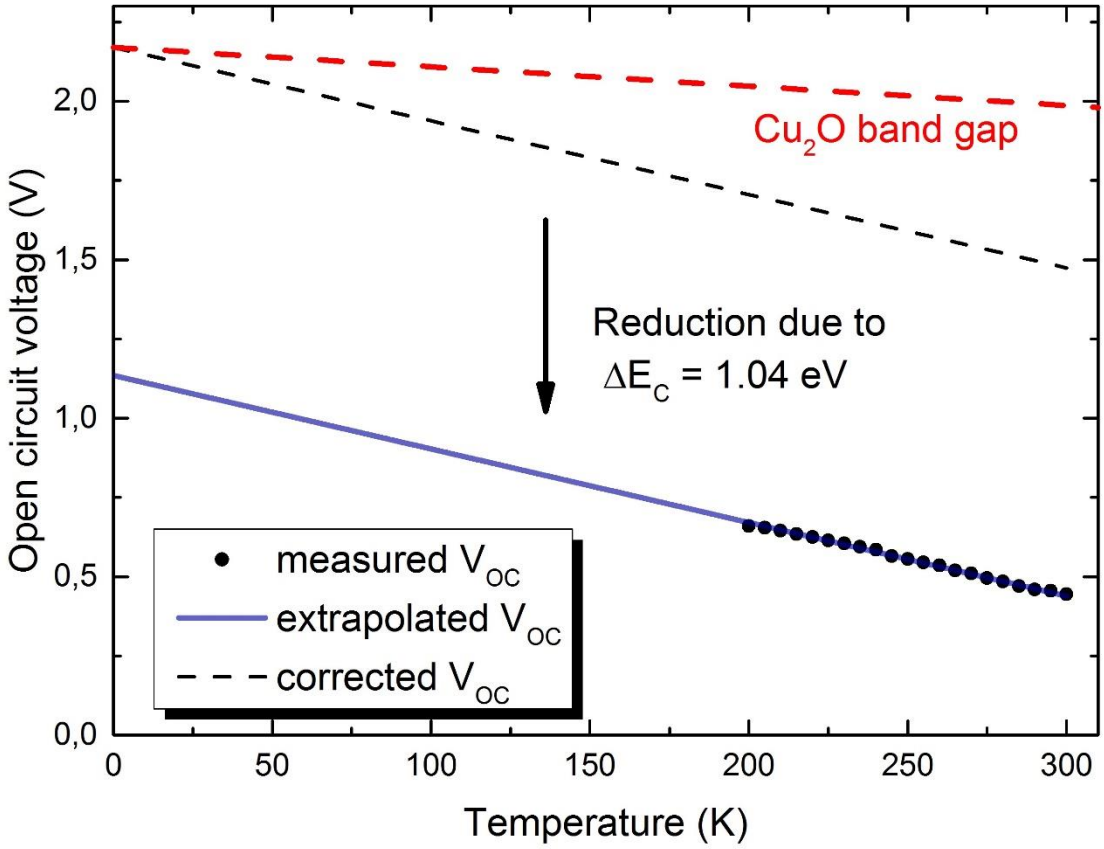

Figure 9: Temperature dependent measurement of the open circuit voltage (black circles), linear extrapolation of the measured open circuit voltage to 0 K (blue line), temperature dependent cuprous oxide band gap energy (red dashed line) and calculated temperature dependent open circuit voltage corrected for the conduction band offset (black dashed line). The open circuit voltage linearly increases with deceasing device operating temperature, which was extrapolated down to 0 K, intercepting the ordinate at the interface band gap of 1.13 eV. In respect to the band gap of cuprous oxide, the conduction band offset is determined to 1.04 eV.

Conclusion

It is demonstrated that alloying gallium nitride with aluminum will increase the attained open circuit voltage when combined with sputter deposited cuprous oxide to form a photovoltaic device. As expected, the short circuit current exhibits just slight changes, which is rendering the heterointerface's recombination velocity, or in other terms, the defect density at the interface as not critical. It is moderate, but not too high. The conduction band offset of $Al_{0.11}Ga_{0.89}N$, the highest aluminum concentration used in this experiment, to cuprous oxide is calculated to be -0.8 eV, which is still too large for optimal performance. Given the miscibility, significantly more aluminum is required to unleash the absorber's full potential in view of the attainable open circuit voltage. Alternatively, one may switch to the gallium oxide material system as window layer and consider to alloy with indium or aluminum to match the conduction band edges. Furthermore, in order to induce the beneficial type inversion in the absorber, the doping profile of the heterojunction requires optimization, i.e., a reduction of the acceptor density in the cuprous oxide absorber and an increase of the donor density in the aluminum gallium nitride window layer by at least one order in magnitude, respectively, is required.

Chapter 3: Cu_2O:H – Passivating Defects

The content of this Chapter is the result of a collaboration with Christian Kandzia, BSc. (Lab assistance), Dipl.-Phys. Benedikt Kramm (SIMS measurements) and Prof. P. J. Klar and has been submitted to peer reviewed scientific journals:

K. P. Hering, J. Benz, C. Kandzia, B. Kramm, M. Eickhoff, and P.J. Klar. *Hydrogen induced mobility enhancement in RF sputtered Cu_2O thin films,* submitted to Advanced Materials

K. P. Hering and P. J. Klar. *Hydrogen induced efficiency enhancement in $Al_{0.11}Ga_{0.89}N/Cu_2O$ solar cells*, submitted to Applied Physics Letters

---

In solar cells using polycrystalline thin films as absorber, grain boundaries can impair the device performance. Several authors reported an improved material's performance of cuprous oxide after hydrogen post-treatments, probably due to a successful defect passivation. [23] [24] [25] [26] [27] The introduction of hydrogen during growth of cuprous oxide, which could possibly render post treatments obsolete and, aiming at photovoltaics, could contribute to cost and conversion efficiency, has not been attempted and investigated yet and is the subject of this Chapter. Polycrystalline Cu_2O thin films were prepared on c-sapphire substrates by reactive radio-frequency sputtering at various temperatures between 500 K and 925 K employing a metallic target and utilizing an argon/hydrogen/oxygen gas mixture. It is demonstrated that the use of hydrogen in the sputter deposition process beneficially affects the transport properties of the Cu_2O films obtained. Correlating the amount of hydrogen incorporated into the thin films, the film morphology and the transport properties demonstrate that in this approach hydrogen is predominantly accumulated at the grain boundaries of the polycrystalline films, leading to a lower film resistivity due the reduction of grain boundary scattering. It is demonstrated that a suitable employment of hydrogen in the growth process of Cu_2O material for solar cell applications improves the material properties significantly.
This finding is then applied to photovoltaics in preparing polycrystalline Cu_2O thin films on $Al_{0.11}Ga_{0.89}N$ templates. It is shown that employing hydrogen in the growth process greatly improves the photovoltaic performance of the heterojunction.

Introduction

Grain boundaries in polycrystalline thin films typically are distinct zones of very high defect densities. Consequently, they are more than likely to host Shockley-Read-Hall recombination at a high rate. Grain boundaries can in principle considered to be similar to the heterojunction interface, and recombination at grain boundaries can be treated in an analogous way. A grain boundary coplanar to the interface constitutes a worst case scenario, when it is located at a position in the absorber where the condition $S_n n = S_p p$ is fulfilled, where S_n and S_p represent the recombination velocities and n and p the free carrier densities, respectively, i.e., the edge of the space charge region in the absorber.

The short circuit current is just weakly affected when the boundary is located within the space charge region, due to the fact that at zero bias holes are not abundant in that region. Under forward bias, however, that changes, resulting in a reduced open circuit voltage and a reduced fill factor. Therefore, grain boundaries inside the space charge region should be avoided, which defines a lower boundary for the grain sizes acceptable in the absorber thin films.

In addition, when charged, grain boundaries induce band bending. Since the Fermi level is located close to the valence band in a p-type semiconducting material, very large acceptor defect densities would be necessary to induce an upward band bending through negative charge. It is much more likely that downward bending occurs by ionized donor-like defects holding positive charge. The latter will introduce a hole repulsing potential barrier. As a consequence, minority electrons are attracted by the grain boundaries, which enhances recombination and reduces the effective diffusion length. Grain boundaries that induce very large band bending may cause an inversion

and form n-channels and thereby shunt the device. The negative influence on a solar cell's performance by grain boundaries can be overcome by attempts to passivate the defects they exhibit, or by increasing the crystallinity.

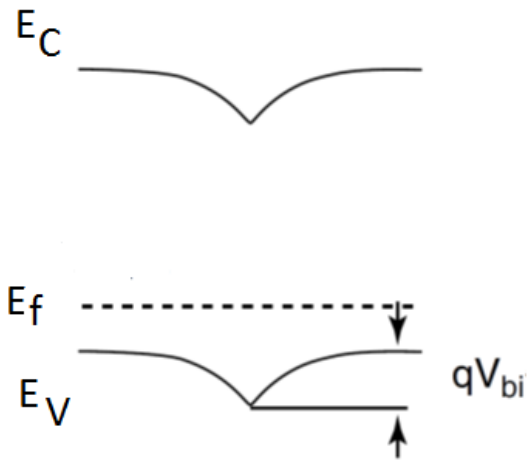

Figure 10: An illustration of the resulting band diagram in p-type semiconductor under the influence of a hole repelling potential barrier, induced by a positively charged grain boundary.

Several authors reported an improved material's performance of cuprous oxide after hydrogen post-treatments, probably due to a successful defect passivation. [23] [26] [25] [27] [24] The introduction of hydrogen during growth of cuprous oxide, which would possibly render post-treatments obsolete and, aiming at photovoltaics, would contribute to cost and conversion efficiency, has not been attempted and investigated yet and is the subject of this Chapter.

Experimental details

The Cuprous oxide thin films were prepared by RF sputtering on c-plane sapphire substrates and n-type $Al_{0.11}Ga_{0.89}N$ templates, $N_d \approx 2E17\ cm^3$, kindly provided by Dr. Armin Dadgar and Prof. Alois Krost. [19] Argon with controlled admixtures of oxygen and hydrogen was used as working gas. The vacuum environment was purged with argon and evacuated to a pressure of at least $5 \cdot 10^{-6}$ mbar prior to deposition. By adjusting the gas flows, the working pressure was set to $8 \cdot 10^{-3}$ mbar and RF power kept constant at 50 W. For the heterostructures, the substrate holder is heated to 925 K The deposition time is chosen to yield film thicknesses of 1 µm. The deposition was followed up by photolithographic structuring, thermal evaporation, and annealing of metal contacts, i.e., Ti/Au for the template and Au for the cuprous oxide absorber, [20], and ultrasonic wire bonding, see Figure 4. Structural characterization was carried out using a Siemens D5000 X-ray diffractometer with a copper anode in Bragg-Brentano configuration. The film thicknesses were obtained from interference oscillations in reflectance spectra, measured by a PerkinElmer Lambda 900 spectrometer. The Secondary Ion Mass (SIMS) measurements were performed using a SIMS MIQ Ion Microprobe from ISA RIBER. The duoplasmatron ion-gun provided a current of 40 nA of 6 keV O_2^- ions focused to an area of $250\ x\ 250\ \mu m^2$ on the sample surface, reaching a mass resolution $m/\Delta m$ of 300. Hole transport properties were investigated by evaluating Hall-effect measurements in Van-der-Pauw geometry. To ensure a decent geometry for highly resistive samples, all of the thin films measured were microstructured by photolithography and etching, creating clover leaf structures. [28] [29] Current-voltage characteristics and external quantum efficiency measurements

were recorded with a Keithley SCS4200 system, Oriel Xe arc lamp and AM1.5 filter, a SPEX 1681B monochromator as well as a Princeton Applied Research 5210 lock-in-amplifier.

Structural properties

Figure 10 depicts the results of the x-ray diffraction (XRD) analysis of series of $Cu_{2\pm\delta}O$ thin films, where the oxygen partial pressure of the working gas in the sputter process was varied, whereas the hydrogen partial pressure was set to zero (no intentional hydrogen added in the growth process). The curves represent the behavior at different substrate temperatures. The diffractograms obtained by XRD, exemplarily shown in the inset, display the position of the (111) reflection is observed in the 2θ range from to 36° to 36.5°. The position observed depends on the oxygen gas flow employed during growth, i.e., it undergoes a shift in angular position as the stoichiometry changes. This effect is more pronounced at lower substrate temperatures where the reflections of the samples grown at the lowest oxygen flow used (about 2.8 sccm) are located at a significantly smaller angle than the reference of $2\theta = 36.419°$ (ICDD PDF No. 00-005-0667) and gradually approach the reference value, which is finally reached for an oxygen flow-rate of about 3.5 sccm. This behavior is indicative for a copper-rich deposition below 3.5 sccm oxygen flow, as well as for residual strain in the thin film. The deviation of the (111) reflections from values in the literature can be avoided by either sputtering at elevated substrate temperatures, e.g. 925 K or 750 K, or by a post deposition anneal at temperatures of 1200 K and above. [8] Thus, by adjusting the reactive oxygen flow, the stoichiometry of the resulting copper oxide thin film can be controlled. The thin films exhibit a weak preferential orientation in the (200) direction. Although the shifted (200) reflection of cuprous oxide almost coincides with the (0002) reflection of the sapphire substrate, it can still be observed by slightly tilting the sample off angle (results not shown here) and is significantly more pronounced than it would be expected when

compared to the intensity relation obtained from the powder diffractogram in the reference measurement. That, in conjunction with the rather broad reflections observed (FWHM > 0.25°), is strong evidence that the degree of crystallinity of the deposited thin films is far from perfection. Scanning electron microscopy (SEM) images of the surfaces of the thin films such as the left image in the top row of images in Figure 15 confirm this supposition. Thus, the diffractograms confirm a successful deposition of $Cu_{2\pm\delta}O$ thin films of a polycrystalline nature. This implies that, in addition to intrinsic defects, grain boundaries are present in the films which will considerably impair charge carrier mobility in the layer and thus performance of solar cells based on such layers.

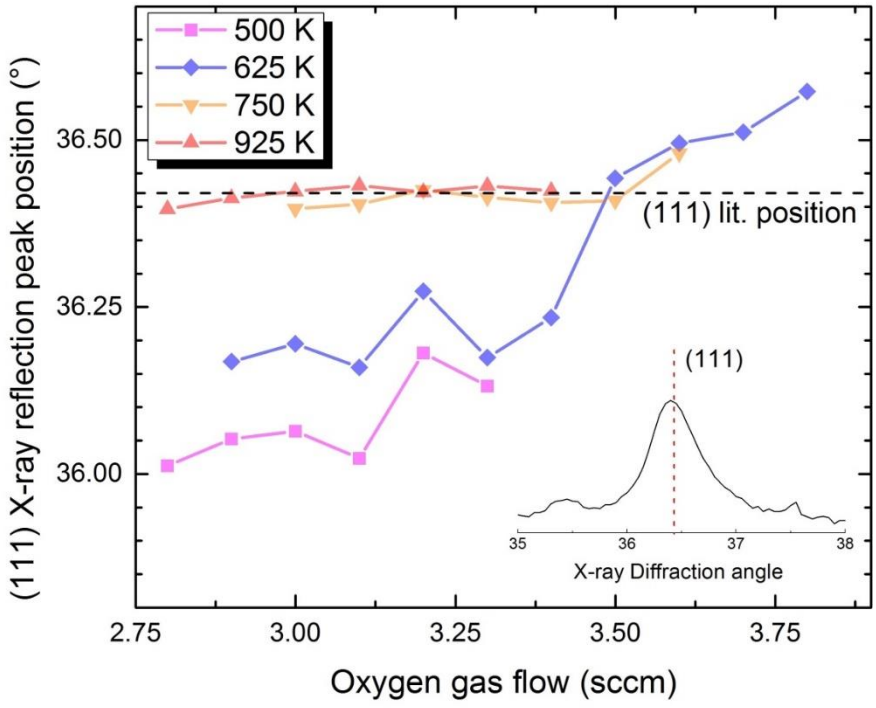

Figure 11: Peak positions obtained for the (111) reflection of the cuprous oxide in the vicinity of 36° as a function of oxygen flow for various substrate temperatures. For lower temperatures the reflections are located at significantly smaller angles, indicating a copper rich deposition of the compound as well as a strained thin film. As the temperature is elevated the position approaches the reference value (dashed line).

Electronic transport properties I

The results of the room-temperature Hall measurements on the series of $Cu_{2\pm\delta}O$ thin films grown at substrate temperatures between 500 K and 925 K are summarized in the left two graphs of Figure 11. As expected, all non-intentionally doped samples show p-type conductivity. The Hall carrier concentrations within the four series show no clear trends, in particular, not for the series of samples grown at 500 K. For the series, grown at 625 K, a weak decrease with increasing oxygen flow is observed which may be explained by an approach of the ideal stoichiometry at an oxygen flow of 3.5 sccm according to Figure 10. The variation of the carrier concentration for the two series grown at 750 K and 900 K is weaker, possibly because the dependence of the stoichiometry on oxygen flow rate is less pronounced, as also suggested by the weaker dependence of the position of the (111) reflection on flow displayed in Figure 10. In contrast, the dependence of the Hall mobility on the oxygen flow of the four series exhibits maxima which become more pronounced with increasing substrate temperature. The oxygen flows corresponding to the maxima are below 3.5 sccm, which means that the corresponding thin films are off stoichiometry and belong to the copper rich regime. The two graphs on the right of Figure 11 summarize results of Hall measurements of cuprous oxide thin films where hydrogen was added during the growth process. The series of samples were grown at the four substrate temperatures of 500, 625, 750, and 925 K. In each series the oxygen flow rate was kept constant at the value where the mobility in the corresponding series without hydrogen was at its maximum and the hydrogen flow was varied between 0 and 0.3 sccm. The presence of hydrogen during the growth process does not have a major impact on the Hall carrier concentration, but significantly

improves the Hall mobilities. All four series exhibit a steady increase of the mobility values with increasing hydrogen flow up to about 0.2 sccm of hydrogen, above this value the mobility declines again.

A direct comparison of the transport parameters of the samples with the highest mobility values grown without adding hydrogen and by adding hydrogen in the growth process is presented in Figure 12. It can be seen that, by adding hydrogen, the Hall mobility may be pushed beyond values that can be reached by merely adjusting stoichiometry, while the charge carrier concentration remains almost unaffected. As a consequence, the samples exhibiting maximum mobility also possess the lowest resistivity. The effect becomes more pronounced at elevated substrate temperatures. The maximum mobility value obtained in this experiment of 88 $\mathrm{cm}^2/\mathrm{Vs}$ approaches values obtained for single crystals. [30]

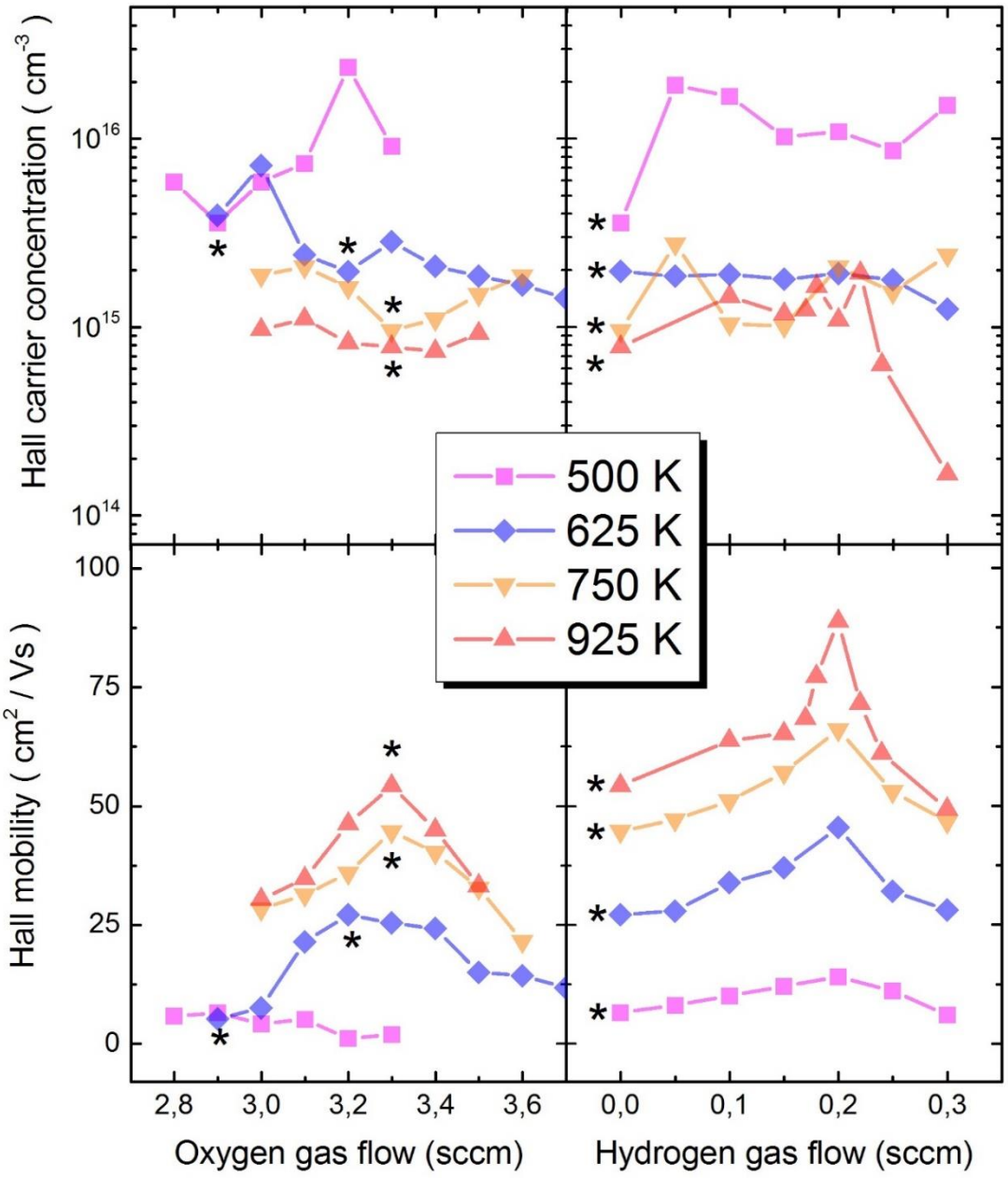

Figure 12: Room-temperature Hall carrier mobility (bottom) and Hall carrier concentration (top) of Cu_2O films in dependence on the applied oxygen (left) and hydrogen gas flow rate (right) during growth for various substrate temperatures. While the carrier concentration is just slightly influenced, the mobilities show maxima depending on the stoichiometry, tuned by the argon/oxygen ratio, and the hydrogen flow rate applied. The fixed oxygen flow rate chosen in the growth of each hydrogen series is indicated by a star.

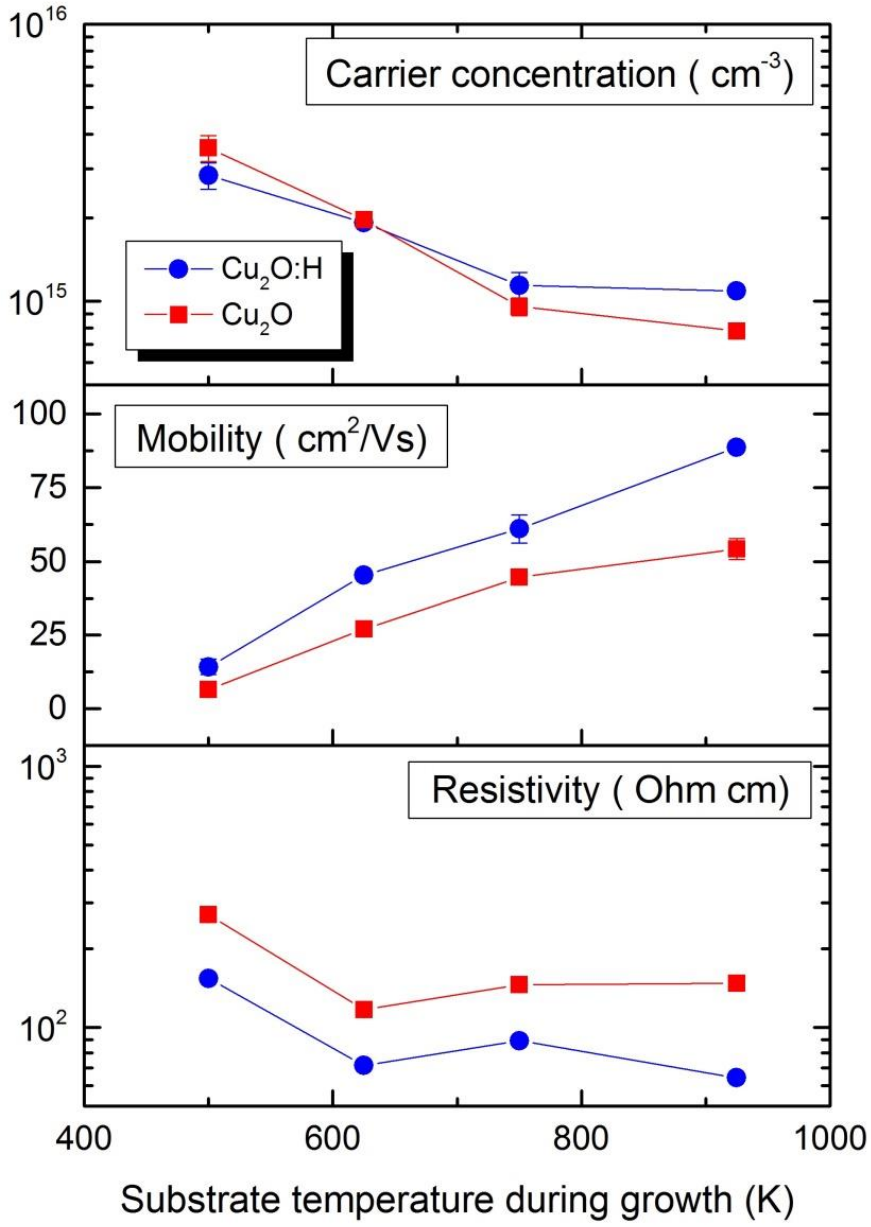

Figure 13: Comparison of the transport properties of the $Cu_{2\pm\delta}O$ thin films of the highest mobility for growth without added hydrogen (red) and growth with added hydrogen (blue) for the four different substrate temperatures. Hall carrier concentration (top), Hall mobility (center) and resistivity (bottom). At all substrate temperatures the majority carrier mobilities increase by adding hydrogen, while the carrier concentration remains almost unaffected, resulting in significantly lower resistivity values for samples where hydrogen was added during growth.

Hydrogen incorporation

To clarify whether hydrogen provided in the growth process is actually incorporated into the film or simply acts as a catalyst, secondary ion mass spectrometry (SIMS) studies on a series of samples grown at different substrate temperatures at an adjusted oxygen flow in the range of 2.8 to 3.5 sccm and at a fixed hydrogen flow of 0.2 sccm was performed. The hydrogen concentrations are derived from SIMS depth profiles. [31] [32] The corresponding data are plotted in Figure 14 and show that the n concentration of incorporated hydrogen decreases with increasing substrate temperature. The almost constant values of $2 \cdot 10^{20}\mathrm{cm}^{-3}$ obtained for substrate temperatures above 600 K are very likely caused by the hydrogen background of the measurement system. Nevertheless, the SIMS analysis confirms the presence of hydrogen in the films. The observed dependence of the incorporated hydrogen concentration on substrate temperature is not easily analyzed, due to the polycrystalline morphology of the thin films. Hydrogen may either be incorporated into the bulk of the grains or be accumulated at the grain boundaries.

The analysis of the transport data gives a first hint which of the two possible locations is preferably occupied by hydrogen, as they are anticipated to affect Hall mobility and Hall carrier concentration in a diametric way. It is theoretically predicted that hydrogen incorporated into the bulk of the Cu_2O grains occupies tetrahedral interstitial sites of the cubic lattice and, in addition, binds copper vacancies in the system in a defect complex which no longer acts as an acceptor, i.e., is a 'hole killer' as Scanlon and Watson named it. [33] This prediction contradicts our experimental findings, as we do not observe a reduction of the Hall carrier concentration when hydrogen is added in the growth

process. A reasonable explanation of the lower carrier mobility at ambient temperature in sputtered thin films compared to bulk crystals is a limitation of the mobility by grain boundary scattering. Thus, it appears likely that an accumulation of hydrogen at the grain boundaries is the cause of the observed increase of mobility, as it has been reported for silicon. [34]

To further verify the hypothesis that hydrogen is primarily accumulated at the grain boundaries, it needs to be taken into account that the thin film morphology varies with growth temperature, in particular, the grain size increases. The average grain size for each sample was determined by analyzing corresponding SEM images; the values are depicted as a second curve in Figure 4. A simple model may be used to analyze the correlation between incorporated amount of hydrogen and grain size. Let us assume that the film surface is square shaped with an edge length d_0 and possesses a thickness t. Furthermore, it should consist of a regular arrangement of columnar grains with a square-shaped cross sections with edge lengths d. An expression for the area consisting of the top and bottom surface of film, its edges, as well as the inner surfaces of the grain boundaries, can be easily derived:

$$A = 2d_0^2 + 2d_0t + 2\frac{d_0^2t}{d}. \quad (3)$$

Since the measured hydrogen concentration is obtained from averaged SIMS depth profiles, where the data of the contaminated top surface and at the film-substrate interface are discarded, both, the top and bottom surface in the model can be disregarded. In the limit of $d << d_0$ one finally obtains the following relationship

between the hydrogen concentration determined by SIMS and the grain size determined by SEM:

$$[\mathrm{H}] = \frac{\sigma\, A}{d_0^2 t} \approx 2\frac{\sigma}{d}, \tag{4}$$

where σ represents the areal density of hydrogen atoms. Therefore, a hyperbolical dependence of the hydrogen concentration on the grain size can be expected, which is indeed confirmed by the experiment, as shown in the inset of Figure 4, where the expression above is fitted to the experimental data, allowing for an offset due to the experimental uncertainty. This analysis yields a realistic value of $\sigma = 9.6 \cdot 10^{15}\ \mathrm{cm}^{-2}$ for the areal density of hydrogen and is a strong hint that hydrogen is mainly incorporated at the grain boundaries of the polycrystalline Cu_2O thin films.

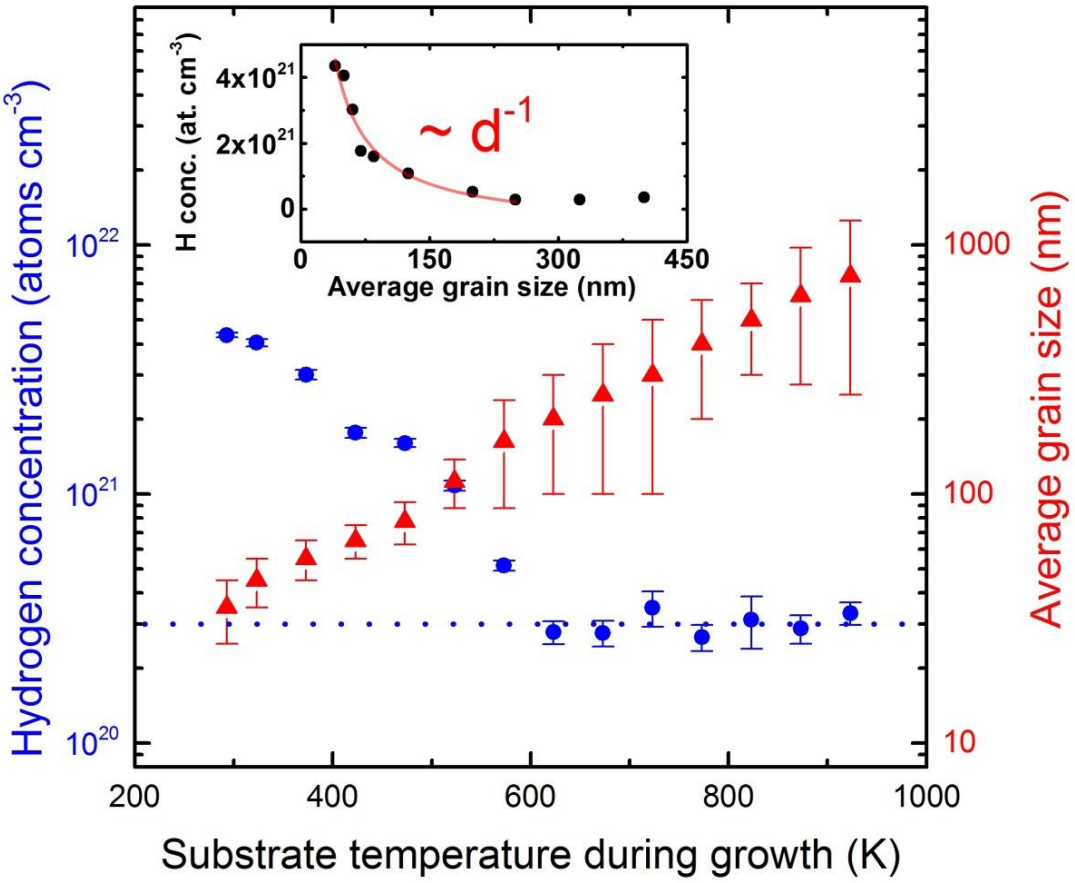

Figure 14: Dependence of the hydrogen concentration (left axis, full circles) and the grain size (right axis, full triangles) on substrate temperature in a series of Cu_2O thin films grown at oxygen and hydrogen flows of 2.8 to 3.5 sccm and 0.2 sccm, respectively. The decrease of the hydrogen concentration with increasing substrate temperature is accompanied by an increase of the grain size. The dotted line represents the detection limit of the SIMS measurement. The inset depicts the resulting hyperbolical dependence of the hydrogen concentration on grain size, indicating that hydrogen is primarily located at surfaces.

Morphological properties

If the effect of hydrogen were only a passivation of the defects at the grain boundaries, the Hall mobility would be expected to steadily increase as grain boundary scattering is the main reason for the lower mobilities in sputtered $Cu_{2\pm\delta}O$ compared to bulk crystals. This is in accordance with the mobility trends observed with increasing hydrogen flow for hydrogen flows up to 0.2 sccm (Figure 2). However, this statement alone cannot explain the drop of the mobility on increasing the hydrogen flow further. The alleged contradiction is resolved by analyzing the variation of the film morphology with increasing hydrogen flow. Figure 15 depicts SEM images of selected samples of the hydrogen series sputtered at 925 K. At zero hydrogen flow, the film surface exhibits grains with sizes of about 200 nm, at low hydrogen flows of 0.05 sccm a smoothing of the surface takes place and the number of grains is reduced. On further increasing the flow, more grains appear again and the grain size increases significantly. Especially for higher hydrogen gas flows, above 0.2 sccm, the average grain size is larger than $1\mu m$. Thin films exhibiting these large grains become more and more disjunctive with increasing hydrogen flow and the disrupted morphology reduces the number of available inter-grain transport paths of the charge carriers probed in the Hall measurements. In the analysis of the Hall data this morphological effect is reflected by an effective decrease of the carrier mobility between 0.2 and 0.3 sccm hydrogen flow. The morphology-induced effect dominates the electrical transport properties for hydrogen flows larger than 0.3 sccm rendering Hall measurements in van-der-Pauw geometry and the corresponding analysis based on the assumption of a homogeneous thin-film inapplicable.

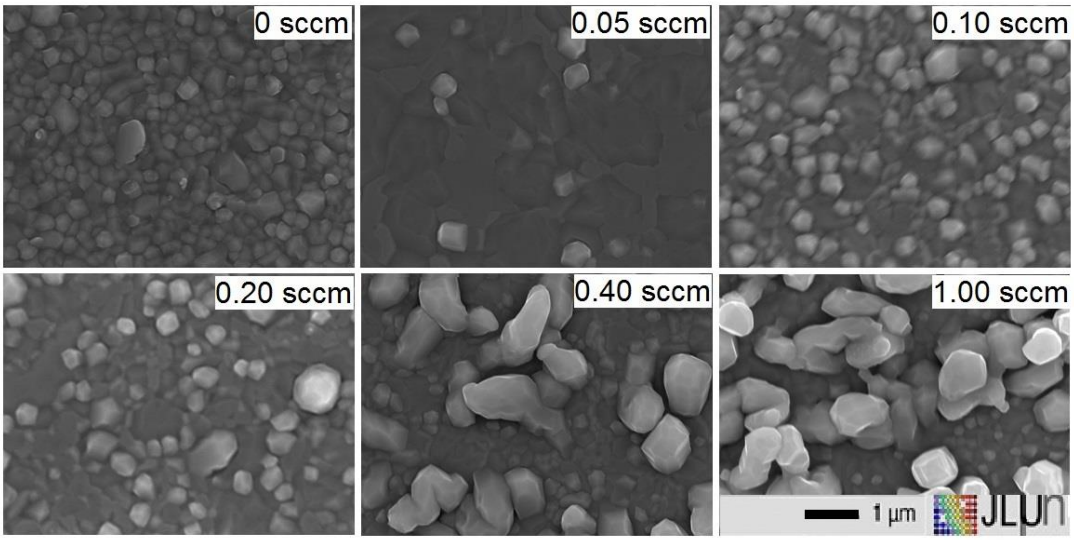

Figure 15: Scanning electron microscopy (SEM) images of the surfaces of Cu_2O thin films sputtered at 925 K using different hydrogen flows in the growth process (increasing from top left to bottom right). The oxygen flow was set to 3.3 sccm. The presence of hydrogen in the growth process strongly influences the film morphology; in particular, large grains and disrupted film morphology are induced at elevated flows.

Electronic transport properties II

In order to gain more insight into the beneficial impact of hydrogen on the mobility we performed temperature-dependent Hall measurements, as the impact of grain boundary scattering is stronger at lower temperatures. An increased grain size as well as a defect passivation affect the mobility in a beneficial way. To study the alleged passivation separately, the measurements were carried out on three samples, where the hydrogen induced morphology-change is negligible. The samples were grown at a substrate temperature of 925 K using hydrogen fluxes of 0, 0.05, and 0.10 sccm, respectively. The Hall data are depicted in Figure 13, on the left hand side the curves of the Hall mobility vs temperature and on the right the curves of the hole concentration vs temperature are displayed. A model of a compensated semiconductor accounting for a single donor and a single acceptor level is used to fit the experimental data. [35] [36]

$$\frac{p(p+N_{\{d\}})}{N_{\{a\}}-N_{\{d\}}-p} = \beta\, N_V \exp\left(-\frac{E_a}{kT}\right), \tag{5}$$

where N_V, N_a, N_d and E_a represent the effective density of states of the valence band, the acceptor density, the donor density and the acceptor binding energy, respectively. Fitting yields acceptor densities $3.2 \cdot 10^{17}, 1.9 \cdot 10^{17}$ and $2.0 \cdot 10^{17}\ \mathrm{cm}^{-3}$, acceptor binding energies of 152, 173 and 220 meV and compensation ratios of 90, 83 and 57% for the samples with 0, 0.05 and 0.1 sccm hydrogen flow applied during growth, respectively. Additional insight is obtained by analyzing the temperature dependence of the Hall mobility of the three samples shown in the left graph of Figure 13. At lower temperatures a much stronger impact of hydrogen on the Hall mobility is observed. Taking into account the scattering mechanisms which limit the mobility in different

temperature regimes, the entire temperature dependence can be modeled as shown in Figure 13. Three scattering mechanisms need to be considered to yield a satisfying agreement between the theory and the experimental data up to room temperature. These are (i) scattering at ionized impurities (dash-dotted curve in the inset of the left graph) as suggested by Lee et al., [37] [38]

$$\mu_{ii} = r_H \frac{128(\epsilon\epsilon_0)^2(kT)^{3/2}\sqrt{2\pi}}{\sqrt{m^*}N_i Z^2 e^3}\left[\ln(1+b) - \frac{b}{1+b}\right]^{-1}, \quad (6)$$

where $b = 24m^*kT/\hbar^2\beta_s^2$ and β_s represents the inverse screening length;

(ii) scattering at grain boundaries (dashed curve in the inset) as modeled by Seto. [39]

$$\mu_{gb} = \sqrt{\frac{q^2L^2}{2\pi\, m^*kT}}\exp\left(-\frac{q\Phi_B}{kT}\right), \quad (7)$$

where L represents the grain size and Φ_B the barrier height; and (iii) as suggested tentatively by Shimada et al. [30] a lowering of the mobility by metastable self-trapping [40] which manifests itself as a pre-factor taking values between 0 and 1 (dot-dash-dotted line in the inset). This latter effect appears to be necessary, since the mobility values predicted by assuming LO phonon scattering to be the dominant scattering mechanism at high temperatures (which is the case in many other materials) are too high. This finding is also in accordance with the results of Lee et al. [38]. Shimada et al. [30] derive the following expression for the pre-factor accounting for the reduction of the mobility by self-trapping

$$\mu_{mst} = \frac{1}{1+\gamma AT^{-3/2}\exp(-E_{mst}/kT)}, \quad (8)$$

where $A = (2\pi\hbar^2/m_p k)/v_0, v_0$ represents the unit cell's volume and γ accounts for degeneracies and entropy changes and E_{mst} describes the depth of the trap.

Combining all three contributions (i) to (iii) yields the Hall mobility which may be compared with the experimental data:

$$\mu(T) = \mu_{mst(T)} \cdot \left(\frac{1}{\mu_{ii}(T)} + \frac{1}{\mu_{gb}(T)}\right)^{-1}. \quad (9)$$

The parameters of the combined expression were deduced by fitting the experimental data of the sample grown at 0.0 sccm H_2. Apart from the potential height Φ_B of the grain boundary barrier and the density of ionized defects which are set to the values extracted from fitting the temperature dependence of the carrier concentrations and the screening length, all these parameters are kept constant in the fitting of the mobility data of the two samples grown by adding hydrogen in the growth process. The agreement between theoretically predicted and experimental Hall data in both graphs is very good at lower temperatures; systematic deviations are observed only for mobility curves at temperatures exceeding room temperature.

The value for the self-trapping energy E_{mst} extracted in this manner is 154 meV, those for Φ_B, are 80, 72 and 64 mV for the samples with 0, 0.05 and 0.1 sccm hydrogen flow applied during growth, respectively. The scattering mechanism limiting the mobility in the high-temperature regime is not clear. Interestingly, the discrepancy at these high temperatures can be removed by another pre-factor of the same form as that already employed (Eq. 6), but with a different value of the trapping energy E'_{mst} = 345 meV, i.e., another type of metastable self-trapping process. The physical origin of such a mechanism is subject to speculation.

The main findings of the model may be summarized as follows: With increasing hydrogen flux at fluxes below 0.2 sccm: (i) the barrier height at the grain boundaries decreases; (ii) the depth of the single acceptor level increases, while the acceptor density decreases; and (iii) the degree of compensation is reduced. The following scenario of the effect of hydrogen in the regime of hydrogen flows below 0.2 sccm is in accordance with our findings. In the untreated sample, there are donors at the grain boundaries, which lead to the high degree of compensation. The Coulomb potential of ionized donor cores determines the barrier height Φ_B at the grain boundaries. The electrons released by the donors cause the compensation of the acceptors. At hydrogen fluxes below 0.2 sccm, hydrogen is mainly incorporated at the grain boundaries of the sputtered Cu_2O thin films, where it passivates the donors, which reduces the degree of compensation and lowers the barrier height Φ_B. The increasing acceptor depth with decreasing compensation cannot be understood in the frame of our simple model for compensation and requires a careful consideration. If the same distribution of acceptor energies was present in all three samples, one would expect that the effective acceptor energy would decrease with decreasing degree of compensation as opposed to an increase. This means that at least two types of acceptors contribute to the distribution of acceptor energies and the resulting hole concentrations observed in the Hall measurements and that this distribution varies with the amount of hydrogen present during the growth process. This suggestion is in accordance with theoretical predictions. In addition to the copper vacancy V_{Cu}, there may be the $V_{Cu,split}$ copper vacancy in split-configuration (which is a slightly different complex where a copper atom adjacent to the vacancy moves to an intermediate site) or even O_i oxygen interstitials. [41] [42] [43] [44] [45] [46] Among the intrinsic acceptors V_{Cu} and $V_{Cu,split}$ theoretically possess the lowest formation energies

followed by the oxygen interstitials (in octahedral and tetrahedral coordination). However, the theoretical values for the acceptor depth of V_{Cu} are between 230 to 280 meV for V_{Cu} and about 470 meV for $V_{Cu,split}$, [43] [45] i.e., both larger than the values extracted from these experiments. An extrinsic acceptor with a smaller acceptor energy of about 160 meV is nitrogen incorporated on oxygen site, N_O. [23] [26] [33] [25] This binding energy is very close to the value obtained experimentally for the hydrogen free sample. The presence of residual nitrogen in the reactor cannot be entirely ruled out. Furthermore, it is likely that the introduction of hydrogen into the reactor affects the formation of N_O and V_{Cu} differently. A preferential formation of V_{Cu} in the presence of hydrogen would be in concordance with the observed trends.

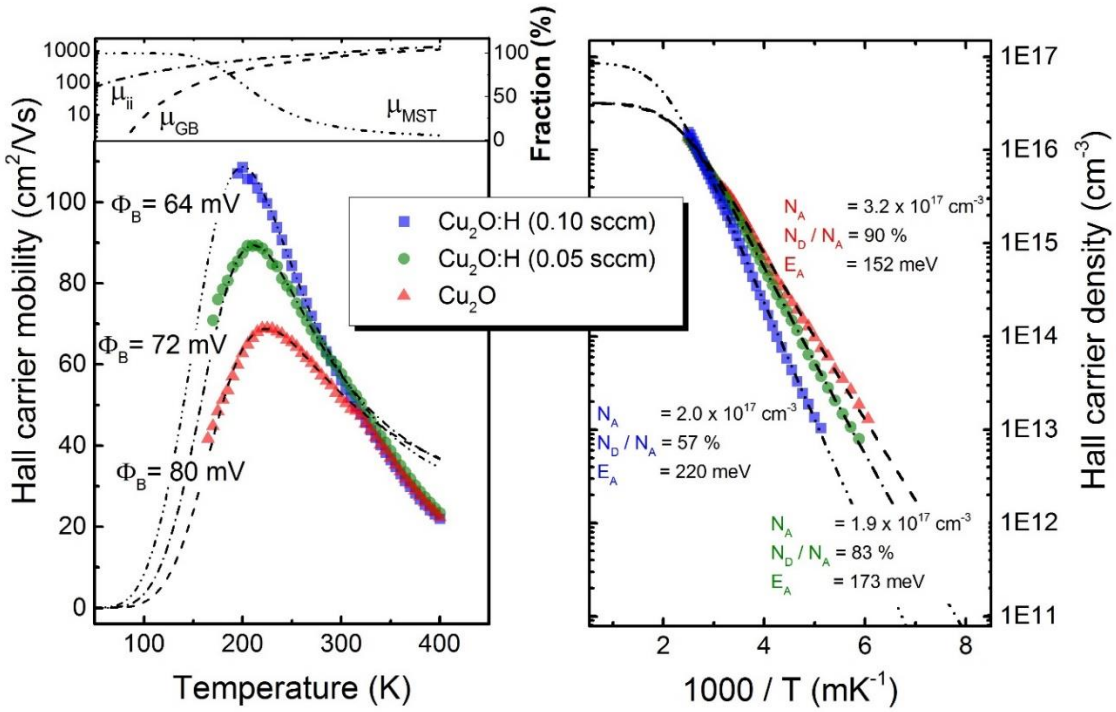

Figure 16: Temperature dependent Hall effect measurements of selected samples grown at a substrate temperature of 925 K, i.e., 0, 0.05 and 0.10 sccm, where the effect of hydrogen induced grain growth is negligible. Depicted on the left is the Hall mobility, which has been modeled as a combination of ionized impurity scattering, metastable self-trapping of holes and scattering at grain boundaries (dashed lines). For each data set all parameters are kept constant except the height of the grain boundary barrier $\mathbf{\Phi_B}$ and the density of ionized defects, which was extracted from fitting the carrier concentrations (right) with the standard model for a compensated semiconductor with a single acceptor (dashed lines). The inset of the left graph depicts the temperature dependence of the contributions of the three dominant scattering processes to the total Hall mobility.

Device characterization

On the left hand side, Figure 16 depicts the results obtained by the external quantum efficiency measurements. When compared, the efficiency of the hydrogenated device is higher for all wavelengths and shows less of a decline at longer wavelengths. That may be explained by the beneficial effect of a hydrogen admixture in the sputtering process on the resulting polycrystalline cuprous oxide thin films. The scattering at grain boundaries is reduced due to defect passivation by hydrogen as discussed in the previous sections. The passivation results in higher majority carrier mobilities in Hall measurements. It may be anticipated that passivated grain boundaries affect the minority carriers in the same manner. Since the diffusion length scales with the minority carrier mobility, the diffusion length will consequently increase as well. However, both efficiencies are low overall and especially for wavelengths exceeding 480 nm. Considering the absorption coefficient of cuprous oxide [8] and the film thickness of 1 µm, the amount of absorbed light should yield much higher values. A comparison between illuminated J-V characteristics of the heterostructure, where hydrogen was employed in the deposition process, and the other, where hydrogen was not present in the deposition process, is depicted on the right hand side of Figure 16. While the open circuit voltage remains constant, the photocurrent is significantly increased and clearly less voltage-dependent when hydrogen was applied, leading to a higher fill factor. Consequently, a higher conversion efficiency of 1.06 % is reached.

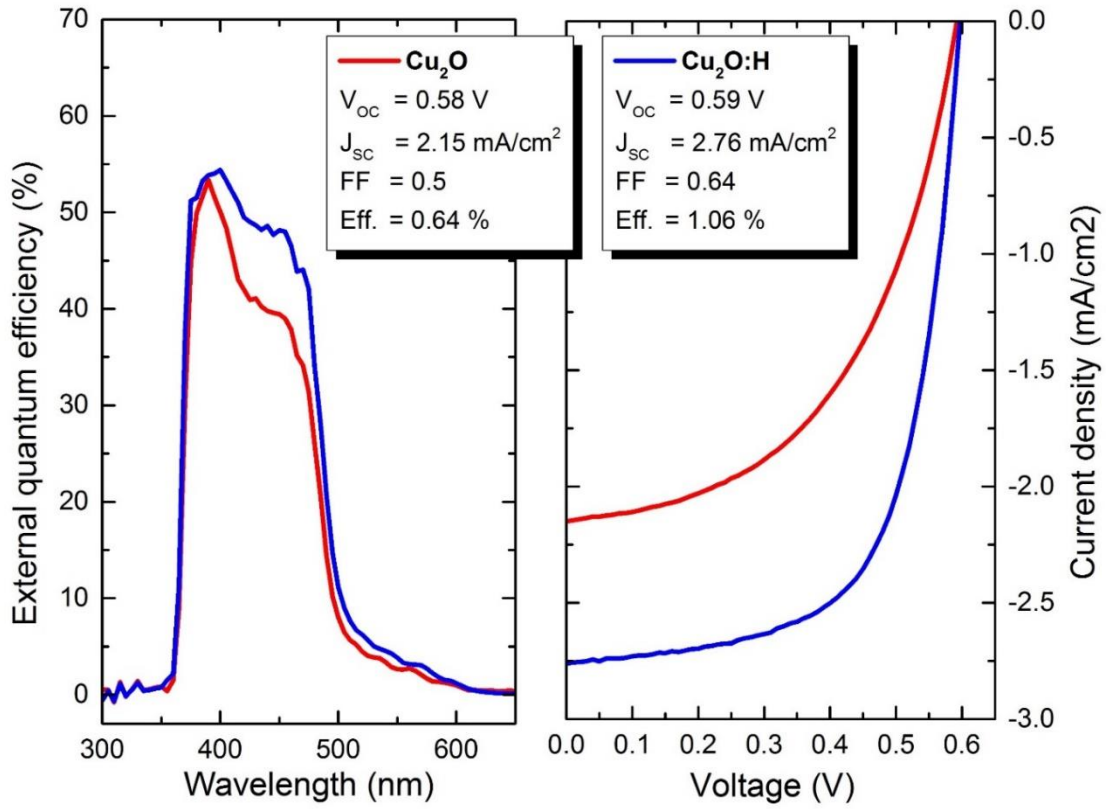

Figure 17: A comparison of the external quantum efficiencies for both, $Al_{0.11}Ga_{0.89}N$ / Cu_2O heterostructures with (blue) and without (red) the application of hydrogen during the copper oxide deposition. (right) A comparison between illuminated J-V characteristics of the heterostructure employing hydrogen in the deposition process (blue) and without the use of hydrogen (red).

The large negative conduction band offset may be held responsible for the discrepancy of low values in the external quantum efficiency present in the entire wavelength range and especially in the blue spectral region, where minority carriers are photogenerated closer to the heterojunction [47] [17]. The reduced open circuit voltage with respect to the band gap of Cu_2O remains unaffected. The influence of the negative conduction band offset was discussed in detail in Chapter 2. The absence of an improvement in the open circuit voltage is explained by the large grain size exhibited at these growth temperatures, which places horizontal grain boundaries outside of the space charge region and only the reduced effective diffusion length affects the quantum efficiency. Characteristic for a low μτ-product is a lowered and voltage-dependent photocurrent in the current-voltage characteristics, which is clearly observed for both of the devices. Upon the employment of hydrogen that effect is significantly reduced, which is in agreement with the observation of the increased quantum efficiency and thus supports that the hydrogen application affects also the minority carriers in a beneficial way.

In order to gain insight into the dominant recombination mechanism under illumination, usually the ideality factor of the standard diode model [16] is evaluated. However, when parasitic resistances and photocurrent are illumination- and voltage-dependent, respectively, the diode model cannot easily be applied, especially for higher forward voltages in the fourth quadrant. For the hydrogenated device that voltage dependence is sufficiently low to allow for an analysis of the illuminated characteristics. Therefore, results for the short circuit current and open circuit voltage at different light intensities were collected by changing the distance from the light source, yielding a partial $J_{sc} - V_{oc}$ curve [48], where the complication due to the effect of series resistance is absent, see Figure 17. Accounting for a shunt resistance, the diode model is fitted to the curve in two

voltage regimes. An ideality factor of 1.89 was derived in the lower voltage regime, which is usually attributed to Shockley-Read-Hall recombination [14] [13] in the space charge region, as the dominating mechanism. At higher voltages, where the space charge region is small, the ideality factor is significantly reduced to 1.36, indicating defect recombination outside the space charge region. However, with the large negative conduction band offset and a high absorber doping, which does not provide a strong doping asymmetry with respect to the window layer, interface recombination is very likely to take place as well. Finally, the model was extended by the introduction of a series resistance and fitted to the illuminated JV characteristics with the ideality factor obtained in the high voltage regime, where the change of the photocurrent due to its voltage dependence is weak. The extracted values for the shunt and series resistance are 8.3 $k\Omega cm^2$ and 8 Ωcm^2, respectively. The diode current in the dark proves to be lower than under illumination at higher forward voltages, which cannot be explained by illumination dependent parasitic resistances alone. That effect, which is sometimes referred to as 'cross over', can be attributed to a potential barrier at the heterointerface. Such a barrier impedes the electron transport across the junction and originates from negative charge at the interface or in its vicinity. Under illumination that barrier may be lowered when the charge accumulated at defects is reduced, which in turn allows for higher currents. [49] [50]

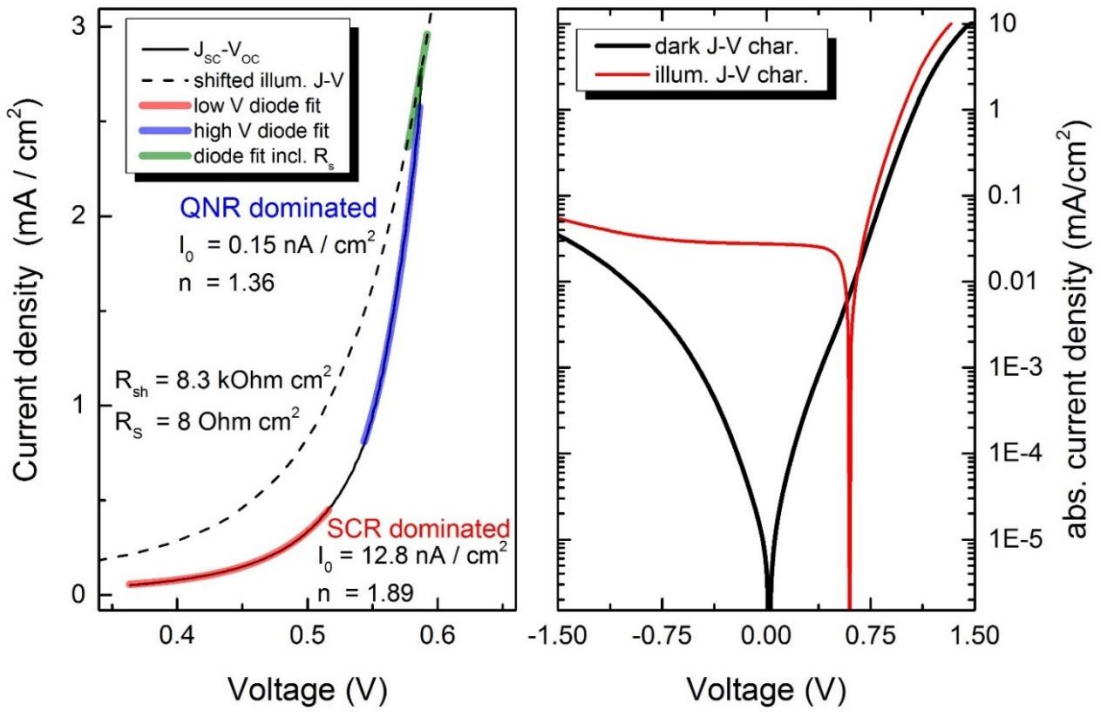

Figure 18: For the device employing hydrogen: (left) $\mathbf{J_{SC} - V_{OC}}$ characteristics (black), illuminated J-V characteristics shifted by a $\mathbf{J_{SC}}$ (dashed), results from curve fitting the diode model without series resistances for a low and high voltage regime to the $\mathbf{J_{SC} - V_{OC}}$ curve (red and blue) and results of fitting the diode model including series resistance and parameters extracted from the high voltage regime to the shifted illuminated J-V characteristics in the range of $\mathbf{V_{OC}}$, where the voltage-dependent change in photocurrent is low and the illumination is close to regular operation condition. (right) J-V characteristics in the dark and under illumination.

Conclusion

It was demonstrated that introducing hydrogen in the sputter deposition process of polycrystalline Cu_2O thin films improves the transport properties of the material considerably. In particular, the Hall mobility may approach values similar to those of bulk crystals, and the hole concentration is only weakly affected. The reason is that in our process hydrogen is not incorporated into the bulk of the grains, but passivates the grain boundaries instead, thus reducing grain boundary scattering. Our results differ to some degree from the findings of other authors who also studied the effect of hydrogen on the properties of Cu_2O. Tabuchi et al. prepared Cu_2O by low-temperature oxidation of sputtered copper thin films. They demonstrated that the transport properties are affected by the use of atomic hydrogen in the oxidation process, but observed a reduction of the carrier concentration accompanied by an increase of carrier mobility. [24] Ishizuka et al. used a post-growth thermal treatment of sputtered Cu_2O:N films with hydrogen and observed an increase of the carrier density in conjunction with a drop in mobility, in total leading to a lower resistivity of films subjected to the post-growth treatment. They suggest that the observed increase in carrier concentration by hydrogen treatment is caused by the H-termination of dangling bonds of Cu at surfaces and interfaces. [26] [27] The various and differing trends observed for the transport properties of Cu_2O, arising from different hydrogen treatments, reflect the complexity of the interplay between the ways, how hydrogen is provided, how the grain morphology of the thin-film sample is affected, and which is the preferred hydrogen site. It is worth noting, that the view expressed by Scanlon and Watson, that the presence of hydrogen should be avoided in Cu_2O material for solar cell applications, may hold for bulk crystalline

material, but does not necessarily hold for polycrystalline Cu_2O thin films. [33] Hydrogen can indeed be beneficial in optimizing the properties of such thin films for use as active material in solar cells and may offer new pathways for raising the cell efficiencies of solar cells based on such films. Furthermore, we demonstrated that the beneficial hydrogen treatment can be part of the sputtering process itself, rather than a post-growth treatment, which avoids an additional process step in device fabrication and, thus, is a contribution to cost effectiveness.

Furthermore, introducing hydrogen in the sputter deposition process improves the photovoltaic conversion performance when applied in a heterostructure. In particular, the quantum efficiency towards longer wavelengths and, consequently, the photocurrent, as well as the fill factor are increased, which can be attributed to an increased diffusion length, due to the reduced scattering at grain boundaries induced by hydrogen. The efficiency of 1.06 % that was reached in this experiment is still considerably lower than the current record efficiencies of Minami et al. [5] and Lee et al. [10], based on thermally oxidized copper sheets and electrodeposited cuprous oxide, respectively. However, when diminishing the conduction band offset for example by the use of Ga_2O_3, similar efficiencies may be reached. Furthermore, an optimization of the sputtering process may yield lower acceptor densities, thus resulting in a more appropriate doping profile in heterojunction devices.

Chapter 4: Semi-transparent electrode – Tuning the plasma

The content of this Chapter is the result of a collaboration with Roman Bergert, BSc. (lab assistance) and Prof. Dr. Slobodan Mitic and has been submitted to a peer reviewed scientific journal:

K. P. Hering, R. Bergert, and S. Mitic. *Enhanced $Al_{11}Ga_{89}N/Cu_2O$ solar cells by a semitransparent electrode*, submitted to Applied Physics Letters

---

There exists a large variety of sputter deposition techniques. One possible modification is the introduction of a semitransparent electrode. This simple metal grid will introduce a possibility to change the plasma potential by DC biasing and, to tune the electron temperature, which controls the plasma chemistry. In fact, it can be used to influence the energy carried by the charged particle towards the substrate, where the film is deposited. Depending on the polarity of the bias, negative and positive charge carrying particles exhibit an increase or decrease in kinetic energy, respectively. In particular, a decrease may be beneficial in order to avoid or minimize damage at the substrate-layer interface. For cuprous oxide deposition and especially heterojunction formation this has not been attempted yet and is subject of this Chapter. Polycrystalline Cu_2O thin films were prepared on c-sapphire substrates and n-type $Al_{0.11}Ga_{0.89}N$ templates by radio frequency sputtering at a temperature of 650 K employing a metallic target, an argon/oxygen gas mixture as well as a biased semi-transparent electrode placed between the target and the substrate. Introducing that grid, the possibility to tune the cuprous oxide thin film properties, especially the morphology, by controlling the electron temperature in the plasma as well as the beneficial effect of a suspected reduction of interface state densities through decreased ion energies in photovoltaic heterostructures is demonstrated.

Introduction

Several authors demonstrated the feasibility to improve the transport properties of sputtered thin films by influencing the plasma chemistry via the control over the electron temperature of the plasma in the deposition process. This control can be achieved by employing a semi-transparent electrode between the target and substrate. In 1972 Taylor et al. [51] proposed using a biased grid to divide the discharge chamber into two regions. Placing the grid between the sputtering target and the substrate holder, the generation region and process region, respectively, are formed. With a sufficiently large mesh number, the electron temperature in the process region can be controlled by applying a DC bias to the grid. In a negatively biased grid low-energetic electrons in the generation region will face an insurmountable potential barrier. Electrons that carry a kinetic energy high enough to pass the barrier will collide with neutral particles in the process region and lose energy in the ionization process. Controlling the electron temperature allows one to control the plasma-chemical reaction by reducing the amount of ionized particles that disturb the reaction, that leads to the deposition of material desired. In reactive sputtering problems may arise from the effect that the grid itself will be coated during deposition. If the material formed on the grid exhibits a high resistivity, the grid itself will no longer be able to maintain the applied DC bias on its surfaces in contact with the plasma. [52] [53] [54] [55] [56] This issue will only become notable when the current between the plasma and DC bias source is limited by the grid coating's resistance instead of the plasma itself. Since cuprous oxide is conductive, very large thicknesses of the deposited cuprous oxide are necessary on the grid to limit that current. To verify this,

the current was monitored in our experiment and was found unchanged throughout any of the depositions carried out.

Experimental details

Using the grid-modified reactive radio-frequency sputter-deposition, cuprous oxide thin films were prepared on polished c-cut sapphire substrates and on n-type $Al_{0.11}Ga_{0.89}N$ templates, $N_d \approx 2E17\ cm^3$, kindly provided by Dr. Armin Dadgar and Prof. Alois Krost. [19] A Dressler 300 W RF generator at 13.54 MHz and 50 W was used to excite the plasma. As cathode material a Kurt J. Lesker Co. Ltd. 5N metallic copper target, 3 inches in diameter was employed. An argon/oxygen gas mixture is used in the sputtering process. After purging with argon, the vacuum chamber was evacuated to at least 5E-6 mbar, before initiating the plasma deposition with 50 sccm Ar and 3.2 sccm O_2. The resulting working pressure was 8E-3 mbar. To establish control over the electron temperature and ion energies a biasable grid was placed between the sputtering target and the substrate holder inside the vacuum chamber, as depicted in Figure 18. The distance between the grid and the substrate holder was chosen to be 10 mm. The distance from the grid to the substrates was reduced to 3 mm by mounting a copper block on to the substrate holder. The substrate holder was heated to result in temperatures of 650 K at the top of the copper block. The aluminum gallium nitride templates were fabricated by MOVPE. [19] For the heterostructures, the deposition time was chosen to yield film thicknesses of 500nm; the deposition was followed up by photolithographic structuring, thermal evaporation and annealing of metal contacts, i.e., Ti/Au for the template and Au for the cuprous oxide absorber [20], as illustrated in Figure 4, and ultrasonic wire bonding. J-V characteristics and external quantum efficiency measurements were carried out with a Keithley SCS4200 system, Oriel Xe arc lamp and AM1.5 filter, a SPEX 1681B monochromator as well as a Princeton Applied Research 5210 lock-in-amplifier.

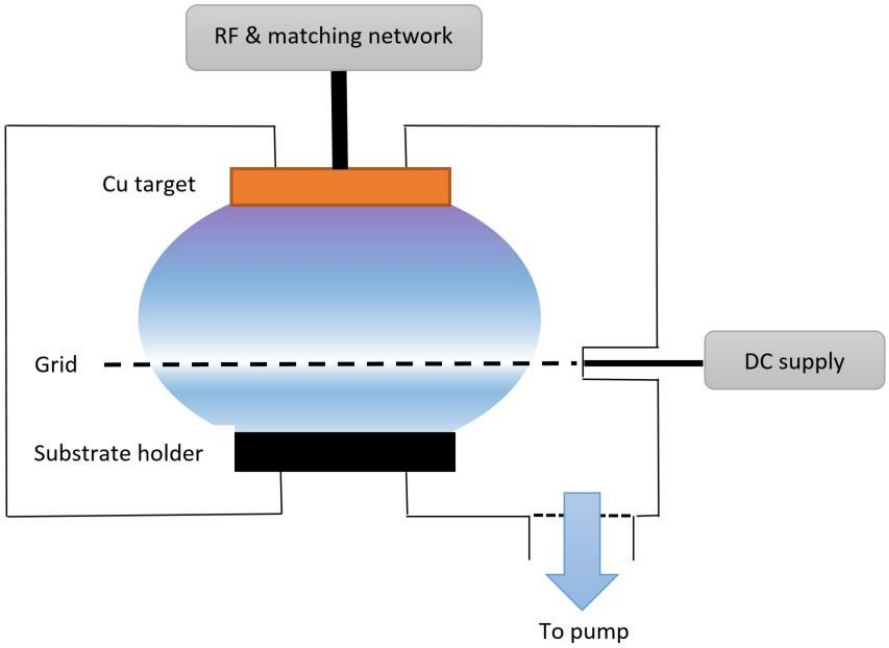

Figure 19: A schematic of the modified deposition setup. The biased grid is located 10 mm above the substrate holder.

Structural properties

Figure 19 depicts the XRD diffractograms in the vicinity of the (111) reflection of a series of cuprous oxide thin films where the bias voltage of the grid was varied from -100 V to 100 V. Up top is the result for a reference sample, grown with no grid present during the deposition. The values of the argon/oxygen gas mixture were set to 50 sccm and 3.3 sccm, respectively. This gas mixture yielded a majority carrier mobility maximum by stoichiometry adjustment at the substrate temperature of 650 K in the 'gridless' deposition, as described in Chapter 3. The position of the reflection slightly deviates from the reference value (ICDD PDF No. 00-005-0667). It is located at smaller diffraction angles, which indicates a deposition in the copper rich regime and may also be a sign for residual stress in the films. The insets on the right hand side show corresponding images of the films' morphologies obtained by scanning electron microscopy. All grid voltages except the setting of -75 V result in significantly lower grain sizes than that of the reference. This finding shows that the electron temperature approaches its optimum for cuprous oxide growth in this setup and for the chosen parameters for a grid bias voltage of about -75 V.

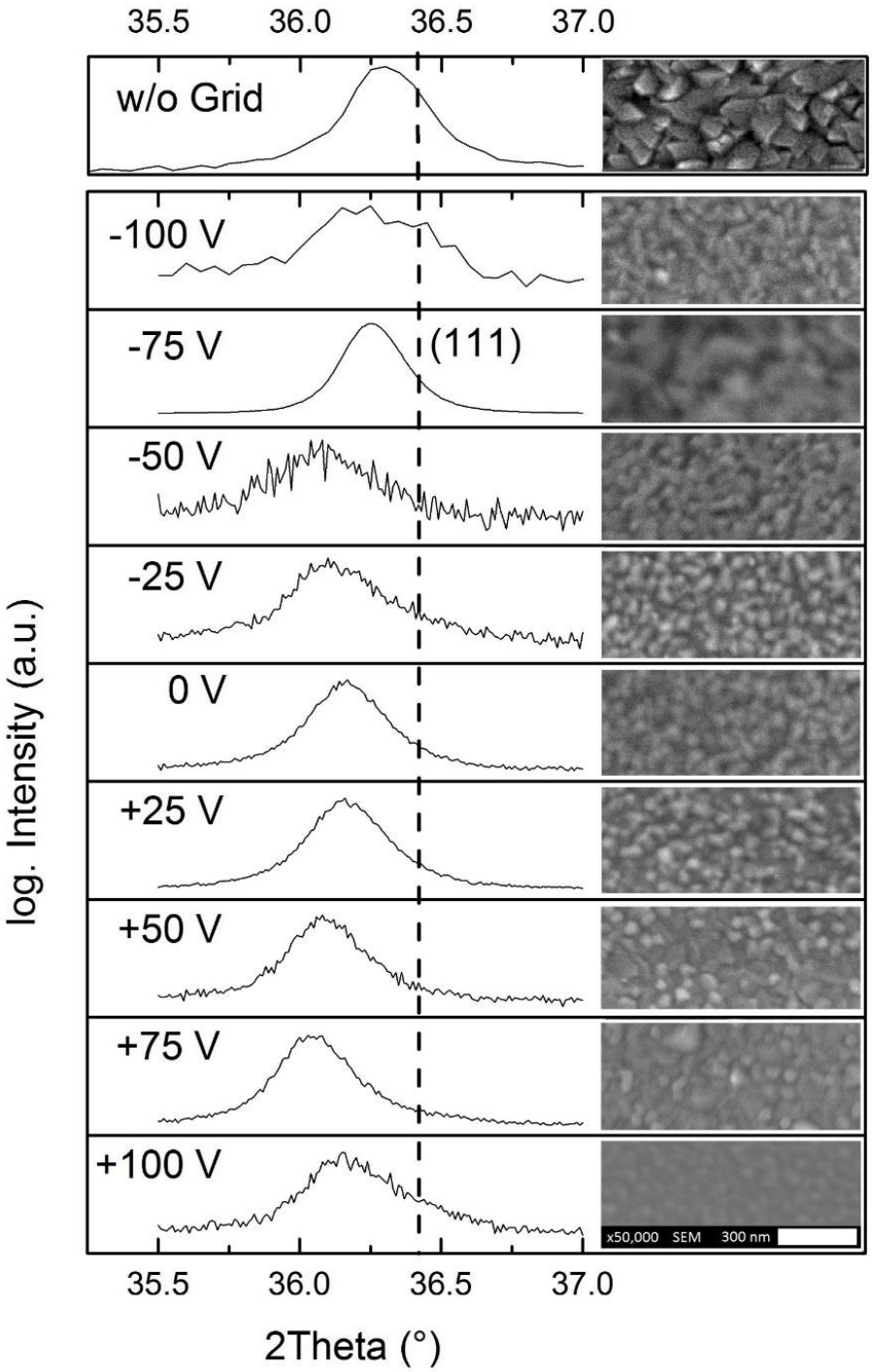

Figure 20: X-ray diffraction results showing the (111) reflection of cuprous oxide in the vicinity of 36° for samples without a grid (top) and with a biased grid present during the deposition. (insets) Corresponding images of the deposited thin films obtained by scanning electron microscopy.

Electronic transport properties and deposition rate

The results of room temperature Hall effect measurements of the samples are shown together with the deposition rate in dependence on the grid voltage in Figure 20. The reference values are given by dashed lines. The carrier concentrations are comparable to the reference and exhibit two maxima, one for each voltage polarity regime of the biased grid. The mobility is significantly lowered compared to the reference. The reason is the reduced grain size and a consequently increased grain boundary scattering. The minimum occurs for a bias voltage of -75 V. It is worth noting that the resistivity of the corresponding sample is lower than that of the reference due to a higher carrier concentration. The resistivity with its minimum corresponds to the mobility maximum. Only the sample grown with a bias voltage set to -75 V shows a mobility comparable to the reference sample. This reflects that both films have a similar grain structure. The deposition rate is decreasing with increasing the grid voltage in a positive sense, indicating that positively charged species in the plasma are the limiting factor in the growth of Cu_2O .

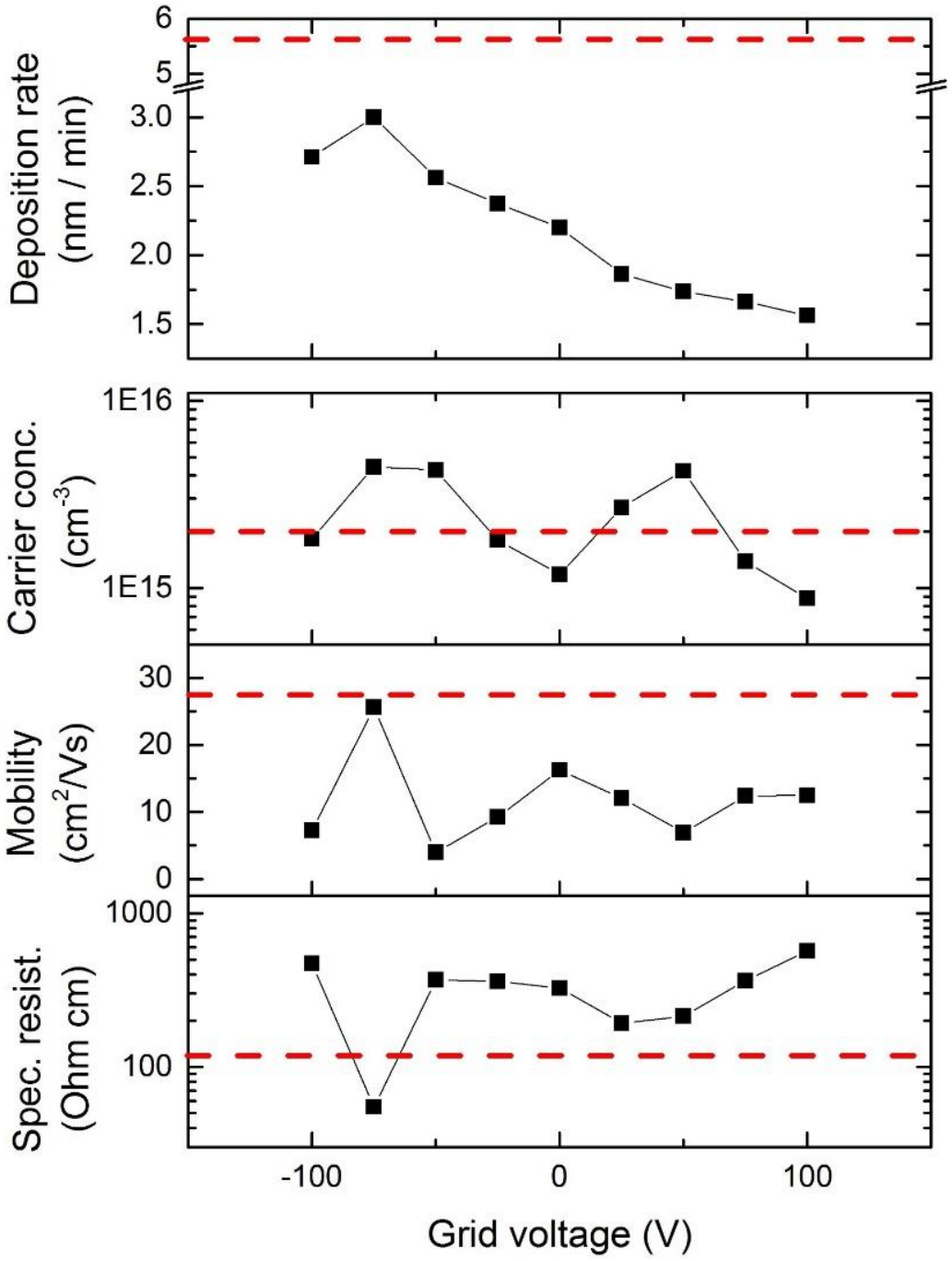

Figure 21: (top:) Results obtained for the deposition rate in dependence on the applied grid bias. The rate is significantly larger when no grid is present (dashed line). (bottom:) Electrical transport properties measured by Hall effect, i.e., carrier concentration, mobility and specific resistivity (top to bottom), of the deposited thin films in dependence on the applied grid bias. Results of the reference sample without a grid are indicated by the dashed lines.

Device characterization

J-V characteristics in the dark and under AM1.5 illumination as well as external quantum efficiency measurements were collected for heterostructures fabricated at different grid bias settings, as shown in Figure 21. The heterostructures are formed by depositing the p-type Cu_2O films on n-type aluminum gallium nitride templates. The quantum efficiencies are overall low with respect to the amount of light absorbed by the cuprous oxide absorber [8]. Interestingly, the quantum efficiencies determined rather show a dependence on the grid bias than on the material properties. Quantum efficiencies and rectification significantly improves for high positive grid voltages as seen on the left of Figure 21 and in the current-voltage characteristics measured in the dark on the top right, respectively. Under full spectrum illumination, the resulting trend of the short circuit currents, which exhibits a significant decrease with decreasing bias voltage is in agreement with the trends observed for the quantum efficiencies, which deteriorate with decreasing bias voltage. The open circuit voltage of all devices is extremely low compared to the band gap of Cu_2O, which is about 2 eV at room temperature. Nevertheless, in terms of short circuit current, the performance of the reference cell grown without a grid present during the deposition is exceeded by the devices created with positive voltages on the grid.

There are several reasons for the overall low quantum efficiencies of these cells. The low quantum efficiencies showing a decline towards longer wavelengths indicate, that the space charge regions do not extend far into the absorber layer. Furthermore, the small grain sizes of the Cu_2O films suggest that there are grain boundaries present within the space charge region. The latter can be held responsible for the low open circuit voltages

and short circuit currents. Moreover, interface recombination is likely to take place, as the conduction band offset is large and negative and the doping profile of the heterostructure too symmetric. Interface recombination has a similar effect on the device performance as small grain sizes. [47] [17] However, the improved performance at positive bias voltages on the grid is a strong indication of a reduction of defect densities at the heterointerface as sputtering damage is reduced. That may be further supported by the fact that sputtering damage enforces the creation of interface defects and is scaling with the kinetic energy of the impinging ions, which are slowed down at positive grid voltages.

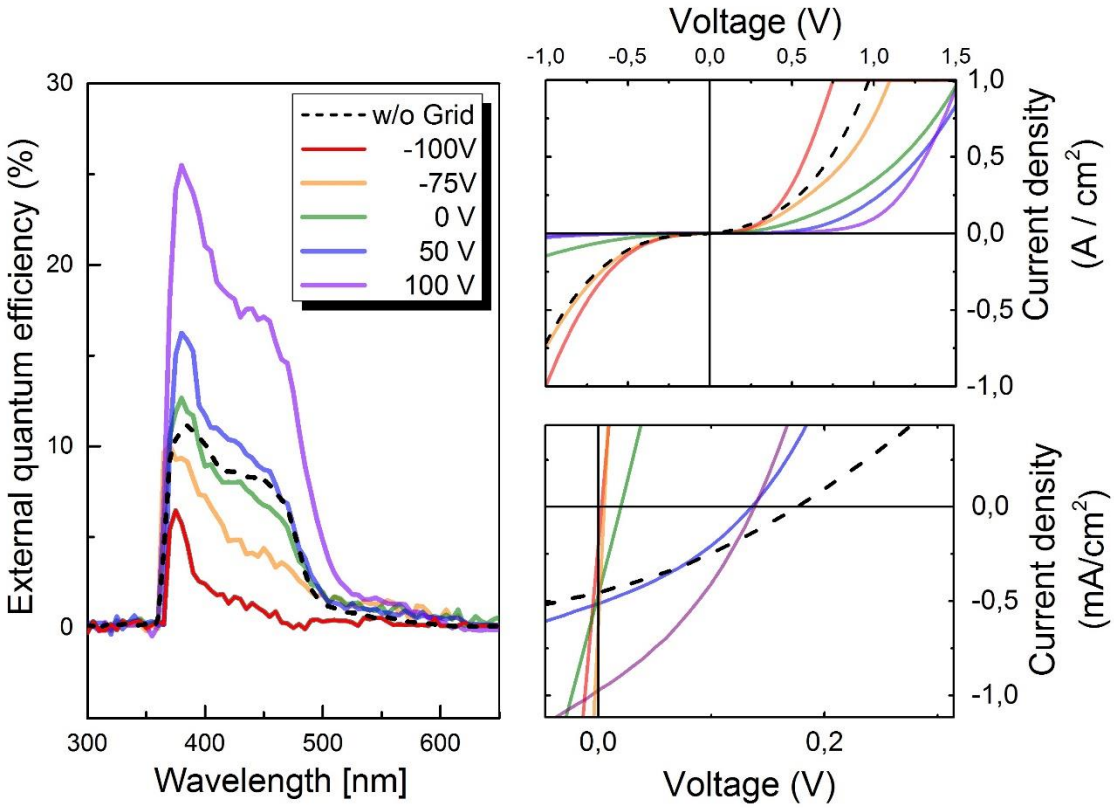

Figure 22: (left:) External quantum efficiency measurements of $Al_{0.11}Ga_{0.89}N$ / Cu_2O heterostructures. The reference is depicted by the dashed line. (top right:) J-V characteristics measured in the dark. (bottom right:) AM1.5 illuminated J-V characteristics in the fourth quadrant.

Despite the fact that the performance of the cells based on cuprous oxide thin films fabricated with the grid technique is not approaching that of the best cell fabricated in the framework of this thesis, the results clearly highlight the importance of the heterointerface quality on the device performance. This becomes obvious by the clear dependence of the quantum efficiency on the grid bias voltage and is further supported by the finding that neither the cell based on the reference thin film without a grid nor the cell based on the film sputtered at -75 V grid bias, that clearly exhibit better Cu_2O bulk properties, but the cell with the heterointerface exhibiting the lowest sputter induced damage (+100 V) shows the highest quantum efficiency.

Plasma potential measurements

The voltages measured by a simple plasma probe, i.e., a copper wire, in dependence on the distance to the grid for several positive bias voltages on the grid are shown in Figure 22. The grid clearly poses a potential barrier for the positively charged species in the plasma and introduces a constant potential step of 25 V, dividing the space between target and grounded substrate holder into two regions with different plasma conditions. Placing the insulating substrates on a copper block beneath but close to the grid, results in voltages on the substrate surfaces close to the grid voltage, therefore the ion energies will be reduced at positive voltages. This effect will be diminished when the distance to the grid is increased, as the ions will be accelerated again and the grid will ultimately just filter low energetic ions.

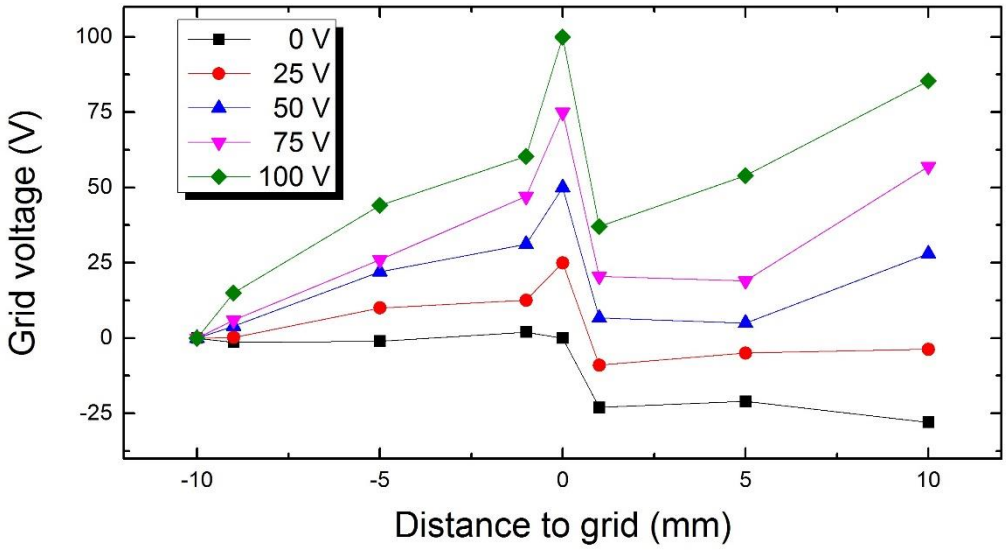

Figure 23: Measured voltage in dependence on the distance to the grid during the deposition process for several positive grid biases. The grid and substrate holder are located at 0 mm and -10 mm, respectively. The voltage curves exhibit a step when crossing the grid.

Conclusion

The successful control of the electron temperature in a capacitive coupled reactive radio frequency sputter deposition process was demonstrated by employing a biased grid between the target and the substrate holder. The ability to tune the material properties of polycrystalline cuprous oxide thin film results. Furthermore, at positive grid voltages the performance of heterojunction solar cells in superstrate configuration is improved compared to cells grown using the same parameters, but no grid. It can be concluded that the devices are limited by interface recombination which can effectively be reduced employing the grid method in the sputter process. The conversion efficiencies observed are not competitive (< 0.1%). However, increasing grain sizes by elevating the substrate temperature during growth, adding hydrogen to the gas mixture used in the sputter deposition process to reduce the grain boundary scattering and employing a window layer which offers a reduced conduction band offset, e.g. Ga_2O_3 [9] [5] [4] [21], should allow one to lift the values in the range of the record efficiencies found in the literature. If a further optimization of the grid-to-substrate distance and corresponding grid bias settings is undertaken, the material properties in view of photovoltaic application may still be improved considerably.

Chapter 5: Cu_2O:N – Tackling the resistivity

Content of this Chapter has been published in a peer reviewed conference accompanying scientific journal:

K. P. Hering, A. Polity, B. Kramm, A. Portz and B. K. Meyer, *Synthesis and characterization of copper oxide compounds*, Materials Research Society Conference Proceedings, Volume 1633, (2014)

Highly efficient solar cells exhibit collection lengths which extend throughout the entire absorber layer, which is thick enough to avoid transmission losses. If this is achieved, a closer a look at the back contact is advised, since it comprises a heterojunction with all complications that may potentially arise. A major issue concerning the heterointerface is the optimization of the doping profile at the interface. For this purpose, obviously an adjustment of the doping in the absorber layer is essential. In this Chapter the ability to vastly increase the conductivity up to the degeneracy of cuprous oxide by extrinsic doping with acceptors, i.e., the introducing nitrogen gas to the deposition process is demonstrated. Since the acceptor density in the sputter deposited cuprous oxide thin films is rather too high, an additionally acceptor doped cuprous oxide layer may not help to reduce the currently limiting effects of interface recombination and low collection length, but it can, in a future perspective, be applied to allow for a reduction in production cost and a more sustainable choice of electrode metal, as well as a viable solution to combat recombination at the back contact by introducing a back surface field and thus suppressing the electron carrier density.

Introduction

In reality, all solar cells exhibit parasitic resistance, i.e., series and shunt resistance. Those resistances will cause losses in terms of photovoltaic conversion. Many circumstances are known to introduce series resistances, e.g. inhomogenities or contact resistances. The latter are introduced when the band bending, present at any metal-semiconductor junction, unless the Fermi levels of both materials coincide, is creating a barrier for the majority carriers of the semiconductor. In view of cuprous oxide, metals with a workfunction larger than 5 eV are needed to avoid this impediment. Unfortunately, not many metals exhibit such large workfunctions and the few that do, e.g. gold or platinum, are scarce and consequently expensive. In the interest of chemical stability, further restrictions to the choice arise. As a way out, one may consider extensive doping of the semiconductor region adjacent to the metal electrodes. Such doping elevates the capacity to screen charge and thus will result in a drastically reduced width of the space charge region in the semiconductor, yielding a reduction of the width of the impeding potential barrier. If done properly, the barrier may then be overcome by tunneling known from basic quantum mechanics. Such a Schottky-contact is sometimes referred to as a tunnel junction. It has been reported that adding nitrogen as a reactive gas during sputter deposition will greatly enhance the conductivity of the resulting cuprous oxide thin films. The suspected underlying mechanism is that nitrogen will be incorporated in the host lattice at an oxygen site, and therefore act as an acceptor [8]. Controlling the defect densities, gives rise to controllling the doping profile of a heterojunction and is key to a successful device operation. Unfortunately, all sputtered cuprous oxide thin films in this thesis already exhibit too high intrinsic acceptor densities. Although doping the cuprous

oxide absorber with nitrogen, which exhibits a smaller activation energy than the intrinsic acceptors, would relocate the Fermi level closer to the absorber's valence band outside of the semiconductor-semiconductor heterojunction's space charge region, which increases the open circuit voltage as desired, however, there are disadvantages. The collection length of the device would be reduced and interface recombination would increase. The resulting losses clearly outweigh the minor gain in V_{OC}. Therefore, doping the complete absorber with nitrogen was not attempted. In view of series resistance however, nitrogen doping of cuprous oxide introduces the possibility to circumvent the restriction of a suitable workfunction for the back metal contact used, basically allowing one to employ any metal as electrode material. The feasibility of this approach has already been successfully demonstrated by Siah et al. [57], who used a metallic copper target in a DC sputtering setup. As the design of the device structures used throughout this thesis comprises a large area back contact, advantages from an improved lateral conductivity by extensive nitrogen doping at the back contact are minor. The recombination path at the heterointerface between the metal back contact and cuprous oxide will only cause losses when the collection length is equal to or greater than the absorber film thickness, which is not the case in our cells. However, in such a case reducing the metal covered area not only leads to a reduced material consumption, but also lowers recombination at the back contact. As demonstrated in the previous chapters, the collection length in our cuprous oxide is significantly lower than the film thickness required to absorb an acceptable portion of the convertible part of the incident light of the solar spectrum. Adding the possibility to create highly doped cuprous oxide to the solar cell fabrication process of this thesis, however, may contribute to production cost efficiency when applied on a large scale. Also, when the collection length of the device

comes near to the metal contact of the absorber, recombination at the semiconductor-metal interface at the back contact may be causing losses. Moreover, the introduction of a thin p+-layer will induce an electric field that repels electrons and thus diminishes recombination at the back contact. Therefore, only the parameter settings necessary to maximize conductivity in the material were explored.

Experimental details

The cuprous oxide thin films were prepared on c-plane sapphire substrates. Argon with controlled admixtures of oxygen and nitrogen was used as working gas. The vacuum environment was purged with argon and evacuated to a pressure of at least $5 \cdot 10^{-6}$ mbar prior to commencing the deposition process. By adjusting the gas flows, the working pressure was set to $8 \cdot 10^{-3}$ mbar and RF power kept constant at 50 W. For the heterostructures, the substrate holder is heated to 500 K. The deposition time is chosen to yield film thicknesses of 1 µm . The film thicknesses were obtained from interference oscillations in reflectance spectra, measured by a PerkinElmer Lambda 900 spectrometer. Hole transport properties were investigated by evaluating Hall-effect measurements in Van-der-Pauw geometry. To ensure a decent geometry, all of the thin films measured were microstructured by photolithography and etching, creating clover leaf structures. [28] [29]

Electronic transport properties

Figure 23 depicts the temperature dependent Hall effect results for a series of cuprous oxide grown at 500 K under the addition of nitrogen. As expected the acceptor densities are largely increased for high nitrogen gas flows and the Hall carrier concentration strongly rises accordingly. By adding nitrogen, the material is starting to develop a defect band and the sign of the Hall coefficient is reversed (not shown), which indicates that the conductivity is dominated by electrons instead of holes, and exhibits a metallic character. The resistivity is reduced by four orders in magnitude in this experiment, which provides more than sufficient conductivity to reduce the area of a metal contact in a solar cell application. The mobilities drop below 1 cm^2/Vs for all nitrogen gas flow settings greater than zero (not shown). The activation energy was extracted from temperature dependent measurements of the resistivity. Due to the broadening of the acceptor band it drops, as the energetic distance of the unoccupied acceptor related energy state to the valence band edge is reduced. For higher nitrogen flows it starts to saturate to a value below 25 meV. The best conducting films obtained by Siah et al. exhibit a higher resistivity than the best obtained in this experiment, i.e., 0.4 Ωcm. This is probably due to a lower carrier density in the films grown by Siah et al. The contact resistivity for different metals in their experiment converges to approximately 1E-4 Ωcm^2. As lower resistivities could be reached in our samples, a reproduction of their results in terms of contact resistance is rendered possible for Cu_2O:N films obtained by our RF sputtering process.

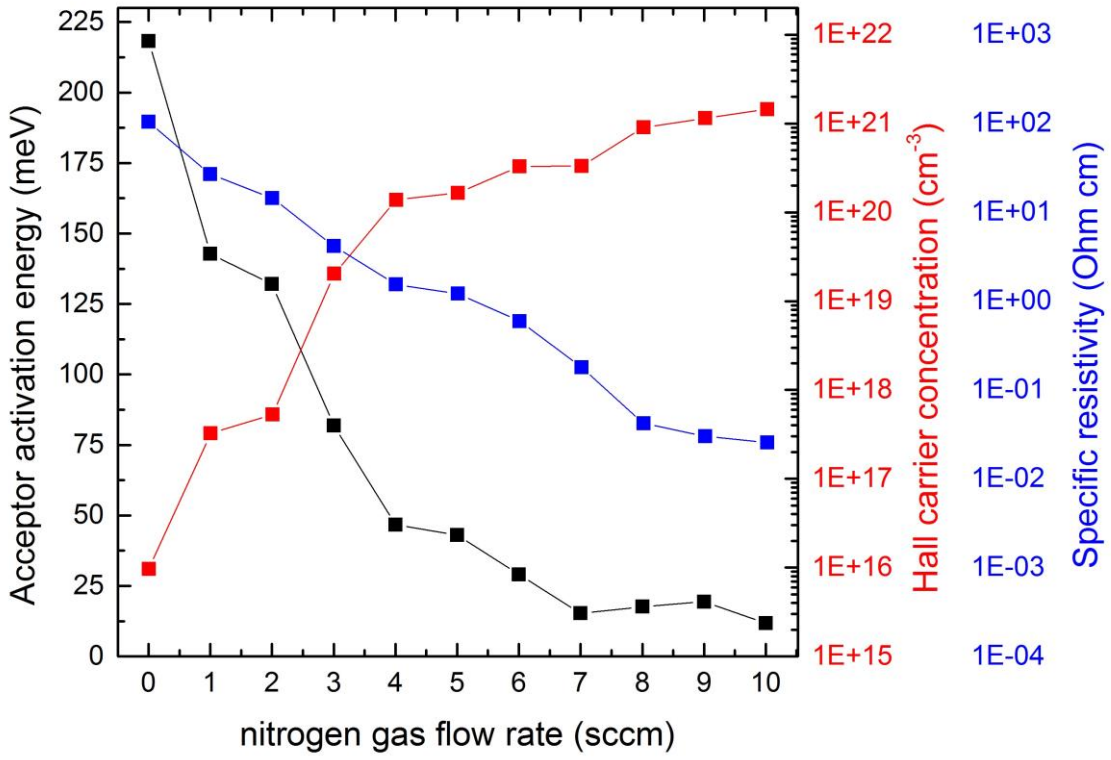

Figure 24: Hall carrier concentration (red), specific resistivity (black) and activation energy (black, determined by temperature dependent measurements) in dependence on the nitrogen gas flow rate applied during deposition. The Hall carrier concentration is increasing and specific resistivity as well as activation energy are decreasing with the nitrogen gas flow rate. The dependencies demonstrate excessive acceptor doping taking place by nitrogen incorporation and at higher nitrogen flows a defect band is beginning to form and the electric transport of the cuprous oxide thin film becomes degenerate.

Conclusion

In conclusion, it was demonstrated that the RF sputter process applied in this thesis can also yield highly degenerate cuprous oxide thin films, so called p^+-layers, which are of interest for photovoltaic device design. An elevation of the acceptor density throughout the cuprous oxide absorber is not advisable, since it will not contribute to a better device performance, but rather impair it.

Chapter 6: Summary and future directions

In this study photovoltaic semiconductor devices based on sputtered cuprous oxide thin films are developed. Several power loss mechanisms are identified and successfully addressed, i.e., a small effective band gap, an enhanced interface recombination, a low collection efficiency of photogenerated charge carriers and parasitic series resistance.

In order to maximize the voltage and current generated by the heterojunction solar cell under illumination, and thus maximize its conversion efficiency, the effective band gap energy at the heterojunction interface has to be equal to the band gap energy of the absorber material. In Chapter 2, it is demonstrated that alloying gallium nitride with aluminum will increase the attained open circuit voltage when combined with sputter deposited cuprous oxide. In the devices, fabricated in the framework of this thesis, the effective band gap energy is reduced by a negative conduction band offset, which is lowered from -1.0 eV to -0.8 eV by alloying with aluminum. The conversion efficiency is increased, but the conduction band offset is still too large to reach the maximum attainable voltage and to significantly reduce the dominant interface recombination exhibited by cuprous oxide absorber based devices.

To further increase the extracted photogenerated current, the collection length in the absorber needs to be sufficiently large. The collection length increases when scattering of charge carriers at, e.g., grain boundaries is reduced. In Chapter 3, it is demonstrated that introducing hydrogen in the sputter deposition process of polycrystalline Cu_2O thin films improves the transport properties of the material considerably. In particular, the Hall mobility may approach values similar to those of bulk crystals, and the hole concentration

is only weakly affected. The reason for this observation is investigated and it is found that a partial passivation of defects at the grain boundaries, reducing grain boundary scattering, takes place. Introducing hydrogen in the sputter deposition process improves the photovoltaic conversion performance when applied in a heterostructure. In particular, the quantum efficiency towards longer wavelengths and, consequently, the extracted photogenerated current, as well as the fill factor, are increased. This results in an increased conversion efficiency of 1.06 % under AM1.5g illumination at 100 mW/cm^2. Thus, hydrogen is beneficial in optimizing the properties of such thin films for use as active material in solar cells and is offering new pathways for raising the cell efficiencies of solar cells based on such films. Furthermore, this demonstrates that the beneficial hydrogen treatment can be part of the sputtering process itself, rather than a post-growth treatment, which avoids an additional process step in device fabrication and, thus, is a contribution to cost effectiveness.

Interface recombination may be reduced by establishing an asymmetric doping profile in the heterojunction device. Aiming at new ways to reduce the intrinsic acceptor density, the successful control of the electron temperature in a capacitive-coupled reactive radio frequency sputter deposition and thereby the ability to control the material properties of polycrystalline cuprous oxide thin films are demonstrated in Chapter 4, by introducing a semitransparent electrode to the sputter deposition process. The modified deposition process neither yields lower acceptor densities nor other desired improvements of the material properties. However, interface recombination originates from defects located at the heterojunction and thus may also be diminished by reducing the interface defect density. At positive grid voltages, relative to the setup's case ground, the performance of

heterojunction solar cells in superstrate configuration, fabricated with this modified deposition method, improves and outperforms a reference cell, fabricated without the semitransparent electrode present during deposition. The improvement is independent of the absorber material properties, and therefore, it may be concluded that the interface defect density is reduced due to a lowered sputter-deposition induced damage, which is inflicted to the underlying aluminum gallium nitride templates. This finding is due to the fact, that at positive voltages on the semitransparent electrode, the potential barrier, it comprises, will reduce the kinetic energy of positively charged species in the plasma, i.e. ions and charged molecules, which impinge on the template surfaces during deposition. The conversion efficiencies observed are not competitive (< 0.1%). However, this finding highlights the importance of sputter-deposition induced damage, which is problematic when sputtering is applied in heterostructure device fabrication. It offers a new way to reduce interface recombination in sputtered heterojunction solar cells, by solving the problem at its core. Consequently, the competitiveness of sputter deposition compared to 'softer' deposition techniques, e.g., atomic layer deposition [10] or pulsed laser deposition [5], is significantly enhanced.

In Chapter 5, it is demonstrated that the sputter process developed in this thesis can also yield degenerate cuprous oxide thin films, so called p+ layers, via a simple nitrogen gas admixture in the sputtering process. Such layers are of interest in photovoltaic device design, as they diminish recombination at the back contact, allow for the introduction of a so called back surface field to the absorber, and for the creation of tunnel junctions, either with basically any back contact metal, or degenerate semiconductor, when applied in a multijunction solar cell structure.

As for future directions, the following is advised:

The negative conduction band offset, exhibited by the devices in the framework of this thesis has to be avoided by all means. Given the miscibility and maintenance of the strong n-type conductivity, significantly more aluminum is required to unleash the absorber's full potential in view of the attainable open circuit voltage. Alternatively, one may switch to the gallium oxide material system as window layer and consider alloying it with indium or aluminum to match the conduction band edges. From this, a relative efficiency increase of at least 100 % can be expected. [21]

Furthermore, in order to induce the beneficial type inversion at the absorber interface, the doping profile of the heterojunction requires optimization, i.e., a reduction of the acceptor density in the cuprous oxide absorber and an increase of the donor density in the window layer by at least one order in magnitude, respectively. Also, lowering the acceptor density in the absorber will lead to an increased collection length, which is currently still insufficient, even despite the hydrogen induced grain boundary passivation, which nevertheless is advised for all future device fabrications.

The highest efficiency of 1.06 %, that was reached in the framework of this thesis, is far behind the current record efficiencies of 6% and 5%, of the cells of Minami et al. [5] and Lee et al. [10], respectively. However, following the directions stated above, similar efficiencies may easily be reached. Furthermore, an optimization in terms of geometry and substrate temperature of the modified sputtering process employing the semitransparent electrode is advised. As interface recombination is the dominant loss mechanism in our photovoltaic devices, reducing it further promises another significant efficiency increase and may allow to achieve new record efficiencies.

References

[1] A. Feltrin and A. Freundlich, *Renewable Energy*, **33**, 180, (2008).

[2] C. Wadia and A. P. Alivisatos, *Environ. Sci. Technol.*, **43**, 2072, (2009).

[3] B. K. Meyer and P. J. Klar, *Phys. Stat. Sol. RRL*, **5**, 318, (2011).

[4] T. Minami, Y. Nishi and T. Miyata, *Appl. Phys. Expr.*, **6**, 044101, (2013).

[5] T. Minami, Y. Nishi and T. Miyata, *Appl. Phys. Expr.*, **8**, 022301, (2015).

[6] T. Minami, Y. Nishi, T. Miyata and J. Nomoto, *Appl. Phys. Expr.*, **4**, 062301, (2011).

[7] A. Mittiga, E. Salza, F. Sarto, M. Tucci and R. Vasanthi, *Appl. Phys. Lett.*, **88**, 163502, (2006).

[8] B. K. Meyer, A. Polity, D. Reppin, M. Becker, P. Hering, P. J. Klar, T. Sander, C. Reindl, J. Benz, M. Eickhoff, C. Heiliger, M. Heinemann, J. Bläsing, A. Krost, S. Shokovets, C. Müller and C. Ronning, *Phys. Stat. Sol. B*, **249**, 1487, (2012).

[9] S. W. Lee, Y. S. Lee, J. Heo, S. C. Siah, D. Chua, R. E. Brandt, S. B. Kim, J. P. Mailoa, T. Buonassisi and R. G. Gordon, *Adv. Energ. Mat.*, **4**, 1301916, (2014).

[10] Y. S. Lee, D. Chua, R.E. Brandt, S. C. Siah, J. V. Li, J. P. Mailoa, S. W. Lee, R. G. Gordon and T. Buonassisi, *Adv. Mater.*, **26**, 4704, (2014).

[11] Y. Liu, H. K. Turley, J. R. Tumbleston, E. T. Samulski and R. Lopez, *Appl. Phys. Lett.*, **98**, 162105, (2011).

[12] K. P. Musselmann, Y. Ievskaya and J. L. MacManus-Driscoll, *Appl. Phys. Lett.*, **101**, 253503, (2012).

[13] W. Shockley and W. T. Read, *Phys. Rev.*, **87**, 835, (1952).

[14] R. N. Hall, *Phys. Rev.*, **87**, 387, (1952).

[15] R. Varache, C. Leendertz, M. E. Gueunier-Farret, J. Haschke, D. Munoz and L. Korte, *Sol. Ener. Mat.Sol. Cells*, **141**, 14-23, (2015).

[16] W. Shockley and H. J. Queisser, *J. Appl. Phys.*, **32**, 510, (1961).

[17] R. Scheer and H.-W. Schock, Chalcogenide Photovoltaics, Weinheim: Wiley, 2011.

[18] B. Kramm, A. Laufer, D. Reppin, A. Kronenberger, P. Hering, A. Polity and B. K. Meyer, *Appl. Phys. Lett.*, **100**, 094102, (2012).

[19] A. Dadgar, J. Bläsing, A. Diez, A. Alam, M. Heuken and A. Krost, *Jpn. J. Appl. Phys.*, **39**, 1183, (2000).

[20] J. Schörmann, P. Hille, M. Schäfer, J. Müßener, P. Becker, P. J. Klar, M. Kleine-Boymann, M. Rohnke, M. de la Mata, J. Arbiol, D. M. Hofmann, J. Teubert and M. Eickhoff, *J. Appl. Phys.*, **114**, 103505, (2013).

[21] R. E. Brandt, M. Young, H. H. Park, A. Dameron, D. Chua, Y. S. Lee, G. Teeter, R. G. Gordon and T. Buonassisi, *Appl. Phys. Lett.*, **105**, 263901, (2014).

[22] J. B. You, X. W. Zhang, S. G. Zhang, J. X. Wang, Z. G. Yin, H. R. Tan, W. J. Zhang, P. K. Chu, B. Cui, A. M. Wowchak, A. M. Dabiran and P. P. Chow, *Appl. Phys. Lett.*, **96**, 201102, (2010).

[23] K. Akimoto, S. Ishizuka, M. Yanagita, Y. Nawa, Goutam, K. Paul and T. Sakurai, *Solar Energy*, **80**, 715-722, (2006).

[24] N. Tabuchi and H. Matsumura, *Jpn. J. Appl. Phys.*, 415060, (2002).

[25] S. Ishizuka, S. Kato, T. Maruyama and K. Akimoto, *Jpn. J. Appl. Phys.*, **40**, 2765, (2001).

[26] S. Ishizuka, S. Kato, Y. Okamoto and K. Akimoto, *J. Cryst. Growth*, **237**, 616-620, (2002).

[27] S. Ishizuka, S. Kato, Y. Okamoto, T. Sakurai, K. Akimoto, N. Fujiwara and H. Kobayashi, *Appl. Surf. Sci.*, **216**, 94-97, (2003).

[28] L. J. Van der Pauw, *Philips Tech. Rev.*, **20**, 220, (1958).

[29] D. C. Look, Electrical characterization of GaAs materials and devices, New York ,NY, USA: Wiley, 1989.

[30] H. Shimada and T. Masumi, *J. Phys. Soc. Jpn.*, **58**, 1717, (1989).

[31] A. Laufer, D. Reppin, H. Metelmann, S. Geburt, C. Ronning, T. Leichtweiss, J. Janek and B. K. Meyer, *Phys. Stat. Sol. B*, **249**, 4, 801-811, (2012).

[32] B. W. Magee and E. M. Botnick, *J. Vac. Sci. Technol.*, 19-47, (1981).

[33] D. O. Scanlon and G. W. Watson, *Phys. Rev. Lett.*, **106**, 186403, (2011).

[34] C. H. Seager and D. S. Ginley, *Appl. Phys. Lett.*, **34**, 337, (1979).

[35] W. H. Brattain, *Rev. Mod. Phys.*, **23**, 203, (1951).

[36] J. S. Blakemore, Semiconductor Statistics, New York, NY, USA: Dover, 1987.

[37] D. Chattopadhyay and H. J. Queisser, *Rev. Mod. Phys.*, **53**, 745, (1981).

[38] Y. S. Lee, M. T. Winkler, S. C. Siah and R. E. B. T. Brandt, *Appl. Phys. Lett.*, **98**, 192115, (2011).

[39] J. Y. W. Seto, *J. Appl. Phys.*, **46**, 5247, (1975).

[40] Y. Toyozawa and A. Sumi, in *Proc. 12th Int. Conf. Phys. Semicond.*, Stuttgart, Germany, (1974).

[41] M. A. Meki-Jeskari, *Model. Simul. Mater. Sci. Eng.*, **14**, 207, (2006).

[42] M. Nolan and S. D. Elliott, *Phys. Chem.*, **8**, 5350, (2006).

[43] H. Räbiger, S. Lany and A. Zunger, *Phys. Rev. B*, **76**, 045209, (2007).

[44] D. O. Scanlon, M. B. J and G. W. Watson, *J. Chem. Phys.*, **131**, 124703, (2009).

[45] D. O. Scanlon, B. J. Morgan and G. W. Watson, *Phys. Rev. Lett.*, **103**, 096405, (2009).

[46] A. F. Wright and N. J. S, *J. Appl. Phys.*, **92**, 5849, (2002).

[47] R. Scheer, *J. Appl. Phys.*, **105**, 104505, (2009).

[48] A. G. Aberle, W. S. R and M. A. Green, in *Proc. IEEE Conf.*, Louisville, Kentucky, USA, (1993).

[49] L. Eisgruber, *Sol. Ener. Mater. Sol. Cells*, **53**, 367, (1998).

[50] A. Niemegeers, M. Burgelman, R. Herberholz, U. Rau, D. Hariskos and H.-W. Schock, in *Prog. Photov. Res. Appl.*, (1998).

[51] R. J. Taylor, K. R. MacKenzie and H. Ikezi, *Rev. Sci. Instr.*, **43**, 1675, (1972).

[52] R. Ikada, G. Nishimura, K. Kato and S. IIzuka, *Thin solid films*, **457**, 55, (2004).

[53] T. Shimizu, S. Iizuka, K. Kato and N. Sato, *Plasm. Sour. Sci. Tech.*, **12**, 521, (2004).

[54] K. Kato, S. IIzuka and N. Sato, *Appl. Phys. Lett.*, **65**, 816, (1994).

[55] J. I. Hong, S. H. Seo, S. S. Kim, N. S. Yoon, C. S. Chang and H. Y. Chang, *Phys. Plasm*, **6**, 3, (1998).

[56] K. H. Bai, C. K. Choi and H. Y. Chang, *Plasma Sour. Sci. Tech.*, **13**, 662, (2004).

[57] S. C. Siah, Y. S. Lee and Y. B. T. Segal, *J. Appl. Phys.*, **112**, 084508, (2012).

[58] Y. S. Lee, J. Heo, S. C. Siah, J. P. Mailoa, R. E. Brandt, S. B. Kim, R. G. Gordon and T. Buonassisi, *Energy Environ. Sci.*, **6**, 2112-2118, (2013).

[59] T. Ito and T. Masumi, *J. Phys. Soc. Jpn.*, **66**, 2185, (1997).

[60] J. Bloem, *Philips Res. Rep.*, **13**, 167, (1958).

[61] L. S. Gorban, I. Yu, I. Gritsenko and S. N. Rud'ko, *Sov. Phys. Sol. State*, **3**, 1559, (1962).

[62] I. Vurgaftman and J. R. Meyer, *J. Appl. Phys.*, **94**, 6, (2003).

[63] J. Teubert, *Private communication.*

Ich erkläre:

Ich habe die vorgelegte Dissertation selbständig und ohne unerlaubte fremde Hilfe und nur mit den Hilfen angefertigt, die ich in der Dissertation angegeben habe. Alle Textstellen, die wörtlich oder sinngemäß aus fremden veröffentlichten Schriften entnommen sind, und alle Angaben, die auf mündlichen Auskünften beruhen, sind als solche kenntlich gemacht. Bei den von mir durchgeführten und in der Dissertation erwähnten Untersuchungen habe ich die Grundsätze guter wissenschaftlicher Praxis, wie sie in der „Satzung der Justus-Liebig-Universität Gießen zur Sicherung guter wissenschaftlicher Praxis“ niedergelegt sind, eingehalten.